Monograph:
Tokhi, M.O. and Azad, A.K.M. (1994) Modelling of a Single-Link Flexible Manipulator System. Research Report. ACSE Research Report 540 . Department of Automatic Control and Systems Engineering

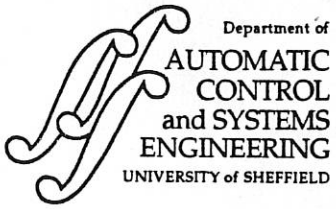

MODELLING OF A SINGLE-LINK FLEXIBLE MANIPULATOR SYSTEM

M O Tokhi and A K M Azad

Department of Automatic Control and Systems Engineering, The University of Sheffield,
P O Box 600, Mappin Street, Sheffield, S1 4DU, UK.

Tel: (0742) 825136.
Fax: (0742) 731 729.
E-mail: O.Tokhi@sheffield.ac.uk.

Research Report No. 540

October 1994

Abstract

This paper presents theoretical and experimental investigations into modelling a single-link flexible manipulator system. An analytical model of the manipulator, characterised by an infinite number of modes, is developed, using the Lagrange's equation and modal expansion method. This is used to develop equivalent time-domain and frequency-domain working models of the system in state-space and transfer function forms respectively. The model parameters are then estimated experimentally using system's measured input/output data. The model thus obtained is validated through experimentation and experimental results including the effect of payload on system characteristics presented and discussed.

Key words: *Flexible manipulator, Lagrange's equation, modal expansion, state-space model, transfer function model.*

CONTENTS

1 Introduction

Research in the area of flexible manipulator systems ranges from single-link manipulator rotating about a fixed axis (Hastings and Book, 1987) to three-dimensional multi-link arms (Nagathan and Soni, 1986). However, experimental work, in general, is almost exclusively limited to single-link manipulators. This is due to the complexity of multi-link manipulator systems, resulting from more degrees of freedom and the increased interactions between gross and deformed motions. The use of dynamic models for flexible manipulator systems are threefold: forward dynamics, inverse dynamics and controller design.

In practice, dynamic models are mostly formulated on the basis of considering forward and inverse dynamics. In this manner, consideration is given to computational efficiency, simplicity and accuracy of the model. Here, a means of predicting changes in the dynamics of the manipulator resulting from changing configurations and loading is proposed, where predictions of changes in mode shapes and frequencies can be made without the need to solve the full determinantal equation of the system. It is important for control purposes to recognise the flexible nature of the manipulator system and to build a suitable mathematical framework for modelling of the system. The flexible manipulator under consideration is a distributed parameter system with rigid body as well as flexible movements. There are two physical limitations associated with the system: (a) the control torque can only be applied at the joint (hub), (b) only a finite number of sensors of bounded bandwidth can be used and at restricted locations along the length of the manipulator.

Owing to the principles used various types of models of flexible manipulator have been developed (Kanoh et al., 1986). These can be classified as

- Lagrange's equation and modal expansion (Ritz-Kantrovitch) or assumed mode method,
- Lagrange's equation and finite element method,
- Euler Newton equation and modal expansion,
- Euler Newton equation and finite element,

- Singular perturbation and frequency domain techniques.

In the Lagrange's equation and modal expansion method, the deflection of the manipulator is represented as a summation of modes. Each mode is assumed as a product of two functions; one dependent on the distance along the length of the manipulator and the other, a generalised co-ordinate, dependent on time. In principle, the summation amounts to an infinite number of modes. However, for practical purposes, a small number of modes is used. The Lagrange's equation and finite element method is conceptually similar to the assumed modes method. Here, the generalised coordinates are the displacement and/or slope at specific points (nodes) along the manipulator (Usoro et al., 1986). The Lagrange's formulation is preferable as its matrix structure readily allows the dynamic model to be reformulated in state-space form. This form is particularly convenient for control purposes.

The Euler-Newton's method is a more direct method of calculating system dynamics. The rate of change of linear and angular momentum are derived explicitly, rather than via Lagrange's equation. Newton's second law is used to balance these terms with the applied forces (Raksha and Goldenberg, 1986). In simulation, or forward dynamics, the linear and angular momentum of the manipulators are the unknowns while the actuator forces are known. Expressing the former in terms of a set of assumed modes of finite elements leads to a dynamic model relating the time dependency of the modes/elements to the external forces. The basic approach in the Euler-Newton and assumed mode method is to divide the manipulator into a number of elements and carry out a dynamic balance on each element. For a large number of elements this is a very tedious process. On the other hand, it is far easier to include non-linear effects without complicating the basic model.

In the singular perturbation technique the system's characteristic modes are separated into two distinct groups: a set of low-frequency or slow modes and a set of high-frequency or fast modes. In the case of flexible manipulators, the rigid-body modes are the slow modes and the flexible modes are the fast modes. The dynamics of the system can then be divided into two sub-systems. The slow sub-system is of the same order as that of the

equivalent rigid manipulator. The slow variables are considered as constant parameters for the fast sub-system.

An alternative to modelling the manipulator in the time-domain is to use a method based on frequency-domain analysis (Book and Majette, 1983). This method develops a concise transfer matrix model using the Euler-Bernoulli beam equation for a uniform beam. The weakness of this method is that it makes no allowance for interaction between the gross motion and the flexible dynamics of the manipulator, nor can these effects be easily included in the model. As a result, the model can only be regarded as approximate.

In this paper an analytical model of a single-link flexible manipulator is first obtained. This is characterised by a set of infinite number of natural modes. This is used to develop a state-space and equivalent frequency-domain models of the system. Three transfer functions are considered, torque to hub angle, torque to hub velocity and torque to end-point acceleration of the manipulator to reflect upon typical sensor measurements available in practical manipulator systems.

Experimental model identification involves estimating a system's transfer function or some equivalent mathematical description of the system from measurements of the system input and output. To ensure the acquisition of high-quality data, an experimental set-up involving a single-link flexible manipulator test rig is designed so that the essential aspects of the measurement process requiring particular attention are considered (Ewins, 1985). These include

- Proper excitation of the structure,
- Choice and location of suitable transducers,
- Selection of conditioning amplifiers and filters,
- Method of signal processing suitable to the system under consideration.

The manipulator is excited and the corresponding input and output signals measured. The input and output signals forming the measured experimental data are used to determine the dynamic characteristics of the system. The characteristics thus obtained are then used to

validate the system model by comparing these with the analytical results of the system model. As the manipulator is very lightly damped, two independent methods are used to extract the natural frequencies. The model parameters include the natural frequencies, damping ratio, hub modal slope coefficient, modal gain of end-point accelerometer and the transfer function of the system. Investigations are also carried out to study the effect of payload on the characteristics of the manipulator. Experimental results thus obtained are presented and discussed.

2 Dynamic equations of motion of the system

The flexible manipulator system under consideration is modelled as a pinned-free flexible beam, with a mass at the hub, which can bend freely in the horizontal plane but is stiff in vertical bending and torsion. The model development utilises the Lagrange's equation and modal expansion method (Hastings and Book, 1987; Korolov and Chen, 1989). The length of the manipulator is assumed to be constant. Moreover, shear deformation, rotary inertia and effect of axial force are neglected.

A schematic representation of the system is shown in Figure 1 where a manipulator with a moment of inertia I_b, hub inertia I_h, a linear mass density ρ and a length of l is considered. The payload mass is M_p and I_p is the inertia associated with the payload. A control torque $\tau(t)$ is applied at the hub of the manipulator by an actuator motor. The angular displacement of the manipulator, in moving in the $POQ-$plane, is denoted by $\theta(t)$. The height of the link is assumed to be much greater than its width, thus, allowing the manipulator to vibrate (be flexible) dominantly in the horizontal direction. The shear deformation and rotary inertia effects are also ignored.

For an angular displacement θ and an elastic deflection u the total (net) displacement $y(x,t)$ of a point along the manipulator at a distance x from the hub can be described as a function of both the rigid body motion $\theta(t)$ and elastic deflection $u(x,t)$ measured from the line OX;

$$y(x,t) = x\theta(t) + u(x,t) \tag{1}$$

To obtain equations of motion of the manipulator, the associated energies are required to be obtained. These include the kinetic, potential and dissipated energies.

The absolute velocity of a point along the manipulator, at a distance x from the hub, can be written as

$$v = \frac{\partial y}{\partial t} = \frac{\partial u}{\partial t} + x\frac{\partial \theta}{\partial t} \tag{2}$$

Note that only small elastic deflection and small angular velocity are considered. As mentioned before the contribution of the rotational moment of inertia to the kinetic energy is neglected. Thus, the kinetic energy of the system can be written as

$$E_k = \frac{1}{2} I_h \dot{\theta}^2 + \frac{1}{2}\int_0^l v^2 \rho dx + \frac{1}{2}\left[v^2\right]_{x=l} M_p \tag{3}$$

Note in equation (3) that the first term on the right-hand-side is due to the hub inertia, the second term is due to the rotation of the manipulator with respect to the origin and the third term is due to the payload mass. Substituting for v from equation (2) into equation (3) yields

$$E_k = \frac{1}{2} I_h \dot{\theta}^2 + \frac{1}{2}\int_0^l \left(\frac{\partial u}{\partial t} + x\dot{\theta}\right)^2 \rho dx + \frac{1}{2} M_p \left(\frac{\partial u}{\partial t} + x\dot{\theta}\right)^2_{x=l} \tag{4}$$

Equation (4) gives the kinetic energy associated with the manipulator.

The potential energy is related to the bending of the manipulator. Since the height of the manipulator under consideration is assumed to be significantly larger that its thickness, the effects of the shear displacements can be neglected. In this manner, the potential energy of the manipulator can be written as

$$E_p = \frac{1}{2} EI \int_0^l \left[\frac{\partial^2 u}{\partial x^2}\right]^2 dx \tag{5}$$

where, E and I are the Young's modulus and the area moment (second moment) of inertia of the manipulator respectively. Note that, in general, there will be motion of the manipulator in the vertical plane as well, in the form of permanent elastic deflections caused by gravitational forces. This effect, however, is ignored by minimising the flexibility of the manipulator in the vertical direction.

In the formulation of the equations of the system, it is required to consider the mechanisms by which energy is absorbed from the structure during its dynamic operation. If the resistance to transverse velocity is represented by $D(x)$, the corresponding damping force is $D(x)\left(\frac{\partial u}{\partial t}\right)^2$. If the resistance to angular velocity at the hub is equal to D_0, the corresponding damping force is $D_0\left(\frac{\partial^2 u}{\partial u \partial t}\right)^2_{(x=0)}$. If the resistance to strain velocity is represented by D_s, the resulting damping moment will be $D_s I\left(\frac{\partial^3 u}{\partial x^2 \partial t}\right)^2$. Therefore, the energy dissipated by the damping moment and force can be written as

$$E_F = \frac{1}{2}\int_0^l D(x)\left(\frac{\partial u}{\partial t}\right)^2 dx + \frac{1}{2}\int_0^l D_s I\left(\frac{\partial^3 u}{\partial x^2 \partial t}\right)^2 dx + \frac{1}{2} D_0\left(\frac{\partial^2 u}{\partial x \partial t}\right)^2_{x=0} \qquad (6)$$

It has been shown that the damping matrix satisfies the orthogonality conditions and thus can be uncoupled in a similar manner as the inertia and stiffness matrices (Clough and Renzien, 1975). To satisfy the mode superposition analysis it is assumed that $D(x) = b_0 \rho a$, $D_s = b_1 E$ and $D_0 = b_0 I_h$ with b_0 and b_1 representing proportionality constants and a the cross-sectional area of the manipulator.

The non-conservative work for the input torque τ can be written as

$$W = \tau\theta \qquad (7)$$

To obtain the equations of motion of the manipulator, the Hamilton's extended principle described by

$$\int_{t2}^{t1}(\delta L+\delta W)dt=0 \tag{8}$$

subject to $\delta\theta=\delta u=0$ at t_1 to t_2, where, t_1 and t_2 are two arbitrary times ($t_1<t_2$) and $L=E_K-E_P$ is the system Lagrangian can be used (Meirovitch, 1970). In the above equation, δW represents the virtual work, $\delta\theta$ represents a virtual rotation and δu represents a virtual elastic displacement. Using equations (4), (5) and (7) the integral in equation (8) can be written as

$$\delta\int_{t_2}^{t_1}\left(E_k-E_p+W\right)dt=$$
$$\delta\int_{t_2}^{t_1}\left[\frac{1}{2}I_h\dot{\theta}^2+\frac{1}{2}\int_0^l\left(\frac{\partial u}{\partial t}+x\dot{\theta}\right)^2\rho dx+\frac{1}{2}M_p\left(\frac{\partial u}{\partial t}+x\dot{\theta}\right)_{x=l}^2-\frac{1}{2}\int_0^l EI\left(\frac{\partial^2 u}{\partial x^2}\right)^2dx+\tau\theta\right]dt=0$$

The rotary inertia and shear deformation are more pronounced at the high frequencies and more influential on the higher modes (Tse et al., 1987). Since investigations have shown that the first two modes are sufficient in modelling the manipulator, thus, the rotary inertia and shear deformation effects can be ignored. Manipulation of the above equation yields the equation of motion of the manipulator as

$$EI\frac{\partial^4u(x,t)}{\partial x^4}+\rho\frac{\partial^2u(x,t)}{\partial t^2}=-\rho x\ddot{\theta} \tag{9}$$

with the corresponding boundary conditions as

$$\begin{aligned}u(0,t)&=0\\ I_h\frac{\partial^3u(0,t)}{\partial t^2\partial x}-EI\frac{\partial^2u(0,t)}{\partial x^2}&=\tau(t)\\ M_p\frac{\partial^2u(l,t)}{\partial x^2}-EI\frac{\partial^3u(l,t)}{\partial x^3}&=0\\ I_p\frac{\partial^3u(l,t)}{\partial t^2\partial x}+EI\frac{\partial^2u(l,t)}{\partial x^2}&=0\end{aligned} \tag{10}$$

and initial conditions as

$$\begin{aligned} u(x,0) &= 0 \\ \frac{\partial u(x,0)}{\partial x} &= 0 \end{aligned} \tag{11}$$

Note in Figure 1 that as line OP' is tangent to the manipulator at the hub, point O, the following can be written

$$\frac{\partial u(0,t)}{\partial x} = 0$$

Using the above condition and equation (1) the following can be obtained

$$\frac{\partial y(0,t)}{\partial x} = \theta(t) \tag{12}$$

Substituting for $u(x,t)$ from equation (1) into equations (9), (10) and (11), manipulating and simplifying yields the governing equation of motion of the manipulator in terms of $y(x,t)$ as

$$EI\frac{\partial^4 y(x,t)}{\partial x^4} + \rho\frac{\partial^2 y(x,t)}{\partial t^2} = 0 \tag{13}$$

with the corresponding boundary conditions as

$$\begin{aligned} y(0,t) &= 0 \\ I_h\frac{\partial^3 y(0,t)}{\partial t^2 \partial x} - EI\frac{\partial^2 y(0,t)}{\partial x^2} &= \tau(t) \\ M_p\frac{\partial^2 y(l,t)}{\partial x^2} - EI\frac{\partial^3 y(l,t)}{\partial x^3} &= 0 \\ I_p\frac{\partial^3 y(l,t)}{\partial t^2 \partial x} + EI\frac{\partial^2 y(l,t)}{\partial x^2} &= 0 \end{aligned} \tag{14}$$

and initial conditions as

$$\begin{aligned} y(x,0) &= 0 \\ \frac{\partial y(x,0)}{\partial x} &= 0 \end{aligned}$$

Equation (13) gives the fourth-order partial differential equation (PDE) which represents the dynamic equation describing the motion of the flexible manipulator. This equation could also be directly obtained by using Newton's law (Breakwell, 1980). The Hamilton's principle, however, is more convenient to use because it automatically generates the appropriate boundary conditions.

3 Mode shapes

Using the assumed mode method (Meirovitch, 1970; Meyer, 1971), a solution of the dynamic equation of motion of the manipulator can be obtained as a linear combination of the product of admissible functions $\phi_i(x)$ and time-dependent generalised co-ordinates $q_i(t)$;

$$y(x,t) = \sum_{i=0}^{n} \phi_i(x) q_i(t) \quad \text{for} \quad i = 0,1,\ldots,n \tag{15}$$

where, the admissible function, ϕ_i, also called the mode shape, is purely a function of the displacement along the length of the manipulator and q_i is purely a function of time and includes an arbitrary, multiplicative constant. The zeroth mode is the rigid-body mode of the manipulator, characterising the so-called rigid manipulator as considered without elastic deflection.

Substituting for $y(x,t)$ from equation (15) into equation (13) and dividing by $\phi_i(x)q_i(t)$ yields

$$\frac{d^4\phi_i(x)}{dx^4}\frac{1}{\phi_i(x)} + \frac{\rho}{EI}\frac{d^2q_i(t)}{dt^2}\frac{1}{q_i(t)} = 0 \tag{16}$$

Equation (16) is satisfied, for arbitrary x and t, only if each term on the left-hand-side is equal to a constant;

$$\frac{d^4\phi_i(x)}{dx^4}\frac{1}{\phi_i(x)} = -\frac{\rho}{EI}\frac{d^2q_i(t)}{dt^2}\frac{1}{q_i(t)} = \beta_i^4 \tag{17}$$

where β_i is a constant. Thus, equation (17) yields two ordinary differential equations as

$$\frac{d^4\phi_i(x)}{dx^4} - \beta_i^4\phi_i(x) = 0 \tag{18}$$

and

$$\frac{d^2q_i(t)}{dt^2} + \omega_i^2 q_i(t) = 0$$

where,

$$\omega_i^2 = \frac{EI}{\rho}\beta_i^4 \tag{19}$$

Let three dimensionless complex numbers λ, ε and η be defined as

$$\begin{aligned} \lambda_i &= \beta_i l \\ \varepsilon &= \frac{I_h}{Ml^2} = \frac{3I_h}{I_b} \\ \eta &= \frac{M_p}{M} = \frac{3M_p l^2}{I_b} \end{aligned} \tag{20}$$

where, M is the mass of the manipulator (ρl). Equation (18) is a fourth-order ordinary differential equation with a solution of the form

$$\phi_i(x) = A_i\sin\beta_i x + B_i\sinh\beta_i x + C_i\cos\beta_i x + D_i\cosh\beta_i x \tag{21}$$

To find the natural frequencies and mode shapes of the system the values of λ_i satisfying the boundary conditions of the undriven manipulator, $\tau = 0$, are determined together with the corresponding values of the coefficients A_i, B_i, C_i and D_i in equation (21). The boundary conditions in equation (14) are more conveniently expressed in matrix form:

$$S(\lambda_i)\begin{bmatrix} A_i \\ B_i \\ C_i \\ D_i \end{bmatrix} = \begin{bmatrix} 0 \\ 0 \\ 0 \\ 0 \end{bmatrix}$$

where,

$$S(\lambda_i) = \begin{bmatrix} -\lambda_i & 1 & \lambda_i & 1 \\ \lambda_i^3 + \lambda_i^5 I_h/\rho & -\lambda_i^2 & -\lambda_i^3 + \lambda_i^5 I_h/\rho & \lambda_i^2 \\ \lambda_i^2 \sin\lambda_i l + \frac{\lambda_i^5 I_p}{\rho}\cos\lambda_i l & \lambda_i^2 \cos\lambda_i l - \frac{\lambda_i^5 I_p}{\rho}\sin\lambda_i l & -\lambda_i^2 \sinh\lambda_i l + \frac{\lambda_i^5 I_p}{\rho}\cosh\lambda_i l & -\lambda_i^2 \cosh\lambda_i l + \frac{\lambda_i^5 I_p}{\rho}\sinh\lambda_i l \\ -\lambda_i^3 \cos\lambda_i l + \frac{\lambda_i^4 M_p}{\rho}\sin\lambda_i l & \lambda_i^3 \sin\lambda_i l + \frac{\lambda_i^4 M_p}{\rho}\cos\lambda_i l & \lambda_i^3 \cosh\lambda_i l + \frac{\lambda_i^4 M_p}{\rho}\sinh\lambda_i l & \lambda_i^3 \sinh\lambda_i l + \frac{\lambda_i^4 M_p}{\rho}\cosh\lambda_i l \end{bmatrix} \tag{22}$$

For non-trivial solutions S must be singular, giving the characteristic equation

$$|S| = 0 \tag{23}$$

Equation (23) can be solved for the values of $\lambda = \lambda_i$ and, hence, ω_i. This requires utilisation of the orthogonality properties of the mode shapes (Meirovitch, 1970). Using equation (21) and the boundary conditions in equation (14) yields

$$\int_0^l M\phi_i(x)\phi_j(x)dx + I_h\phi_i'(0)\phi_j'(0) + M_p\phi_i(l)\phi_j(l) + I_p\phi_i'(l)\phi_j'(l) = I_T\delta_{ij} \tag{24}$$

where, δ_{ij} is the Kronecker delta and the normalisation constant I_T is the total inertia about the motor armature. Equation (24) uniquely defines the magnitude of the mode $\phi_i(x)$. From the properties of self-adjoint systems, the mode shapes must also satisfy the orthogonality condition

$$\int_0^l EI\phi_i''(x)\phi_j''(x)dx = I_T\omega_i^2\delta_{ij} \tag{25}$$

The analytical values of natural frequencies ω_i can thus be obtained using equations (19) and (20). The ε given in equation (20), as described by the ratio of the hub inertia to

the manipulator's moment of inertia, determines the vibration frequencies of the manipulator; a small ε corresponds to the manipulator having lower vibration frequencies. For a very large ε the vibration frequencies correspond to those of a cantilever beam. The effect of a payload mass, on the other hand, is significant on the vibration frequencies. By considering the boundary conditions the mode shape function $\phi_i(x)$ of the manipulator in equation (21) can be obtained.

4 State-space model

The motion of the flexible manipulator driven by a general torque input, $\tau(t)$, can be modelled using the results of the previous section together with Lagrange's equation. In the absence of an external torque equation (9) can be written as

$$EI\frac{\partial^4 u(x,t)}{\partial x^4}+\rho\frac{\partial^2 u(x,t)}{\partial t^2}=0 \tag{26}$$

Equation (26) represents the behaviour of the manipulator in free transverse vibration, where $u(x,t)$ is the elastic deflection, in the horizontal plane, of a point x along the manipulator at time t. In a similar manner as before, the solution $u(x,t)$ of this equation can be expressed as

$$u(x,t)=\sum_{i=1}^{n} q_i(t)\phi_i(x) \quad \text{for } i=1,2,\cdots,n \tag{27}$$

Replacing u in equations (4) and (5) by the summation in equation (27), and using the orthogonality properties in equations (24) and (25), the kinetic energy E_K and potential energy E_P of the system, in terms of the natural modes, can be obtained as

$$E_K=\frac{1}{2}\delta_{ij}I_b\sum_{i=1}^{n}\dot{q}_i^2 \tag{28}$$

$$E_P=\frac{1}{2}\sum_{i=1}^{n}\sum_{j=1}^{n}q_iq_j\int_0^l EI\phi_i'\phi_j''dx=\frac{1}{2}\delta_{ij}I_t\sum_{i=1}^{n}\omega_i^2q_i^2 \tag{29}$$

Similarly, using equations (6) and (7) the dissipated energy E_F and the work W can be obtained as

$$E_F = \frac{1}{2}(I_h + I_b)2\xi_i\omega_i^2 q_i^2 \tag{30}$$

$$W = \tau\sum_{i=0}^{n}\phi'(0)q_i \tag{31}$$

where $\xi_i = \frac{b_0}{2\omega_i} + \frac{b_1\omega_i}{2}$ is the damping ratio.

The dynamic equation of the system can now be formed using the kinetic energy, potential energy and dissipated energy in the Lagrangian of the energy expression given as (Tse et al., 1987)

$$\frac{d}{dt}\left(\frac{\partial L}{\partial \dot{q}_i}\right) - \frac{\partial L}{\partial \dot{q}_i} + \frac{\partial E_F}{\partial \dot{q}_i} = W_i \tag{32}$$

where, q_i represents the time-dependent generalised co-ordinates and W_i represents the work done by the input torque at the joint in each co-ordinate.

Substituting for E_K, E_P, E_F and W from equations (28), (29) (30) and (31) into equation (32) and using the orthogonality relations in equations (24) and (25), an infinite set of decoupled ordinary differential equations are obtained as

$$\begin{aligned}
\ddot{q}_0 &= \frac{\tau}{I_T} \\
\ddot{q}_1 + 2\xi_1\dot{q}_1 + \omega_1^2 q_1 &= \frac{d\phi_1(0)}{dx}\frac{\tau}{I_T} \\
\ddot{q}_2 + 2\xi_2\dot{q}_2 + \omega_2^2 q_2 &= \frac{d\phi_2(0)}{dx}\frac{\tau}{I_T} \\
&\vdots
\end{aligned} \tag{33}$$

In this manner, due to the distributed nature of the system, there will be an infinite number of modes of vibration of the flexible manipulator that can be represented. However, in practice, it is observed that the contribution of higher modes to the overall movement is negligible. Therefore, a reduced-order model incorporating the lower (dominant) modes is preferred. Retaining, the first $n+1$ modes of interest, equation (33) can be written in a state space form as

$$\frac{dX}{dt} = \mathbf{A}X + \mathbf{B}\tau \tag{34}$$

where,

$$X^T = \{q_0 \quad \dot{q}_0 \quad q_1 \quad \dot{q}_1 \quad \cdots \quad q_n \quad \dot{q}_n\}$$

$$\mathbf{A} = \begin{bmatrix} 0 & 1 & 0 & 0 & 0 & 0 & \cdots & 0 & 0 \\ 0 & 0 & 0 & 0 & 0 & 0 & \cdots & 0 & 0 \\ 0 & 0 & 0 & 1 & 0 & 0 & \cdots & 0 & 0 \\ 0 & 0 & -\omega_1^2 & -2\xi_1\omega_1 & 0 & 0 & \cdots & 0 & 0 \\ 0 & 0 & 0 & 0 & 0 & 1 & \cdots & 0 & 0 \\ 0 & 0 & 0 & 0 & -\omega_2^2 & -2\xi_2\omega_2 & \cdots & 0 & 0 \\ \vdots & \vdots & \vdots & \vdots & \vdots & \vdots & \cdots & \vdots & \vdots \\ 0 & 0 & 0 & 0 & 0 & 0 & \cdots & 0 & 1 \\ 0 & 0 & 0 & 0 & 0 & 0 & \cdots & \omega_n^2 & -2\xi_n\omega_n \end{bmatrix}$$

$$\mathbf{B}^T = \frac{1}{I_T}\left\{0 \quad 1 \quad 0 \quad \frac{d\phi_1(0)}{dx} \quad \cdots \quad 0 \quad \frac{d\phi_n(0)}{dx}\right\}$$

Let the manipulator be facilitated with three sensors; end-point acceleration sensor, hub velocity sensor, and hub angle sensor. The output vector Y of these sensors is related to the state vector by

$$Y = \mathbf{C}X \tag{35}$$

where,

$$\mathbf{C}=\begin{bmatrix} 1 & 0 & \dfrac{d\phi_1^2(l)}{dx^2} & 0 & \cdots & \dfrac{d\phi_n^2(l)}{dx^2} & 0 \\ 1 & 0 & \dfrac{d\phi_1(0)}{dx} & 0 & \cdots & \dfrac{d\phi_n(0)}{dx} & 0 \\ 0 & 1 & 0 & \dfrac{d\phi_1(0)}{dx} & \cdots & 0 & \dfrac{d\phi_n(0)}{dx} \end{bmatrix}$$

with $\frac{d^2\phi_i(l)}{dx^2}$ representing the end-point acceleration sensor modal gain and $\frac{d\phi_i(0)}{dx}$ the actuator (motor) modal gain. It follows from the above that due to the distributed parameter nature of the manipulator system a full-order model will require an infinite number of ordinary differential equations incorporating an infinite number of modal coordinates and mode shapes. Practically, a finite number of modes can be assumed (Kanoh et al., 1986; Cannon and Schmitz, 1984; Hughes, 1987). This assumption is justified by the fact that the dynamics of the system are dominantly governed by a finite number of lower modes.

5 Transfer function model

For frequency domain control design, input/output relationships are usually expressed in a transfer function form. This allows the use of classical design methods, such as Bode plots, Nyquist diagrams and root loci.

The open-loop transfer function of the system, $G(s)$, is given by the ratio $Y\tau^{-1}$. Using the state-space equations, (34) and (35), this can be obtained as

$$G(s)=\mathbf{C}(s\mathbf{I}-\mathbf{A})^{-1}\mathbf{B}$$

where, $\mathbf{I}$ is the identity matrix of the same dimension as $\mathbf{A}$, and s is the Laplace transform variable. Using an alternative method (Breakwell, 1980), the transfer function

can be obtained directly using equation (13). Taking the Laplace transforms of this equation yields the ordinary differential equation

$$EI\frac{d^4\bar{y}(x,s)}{dx^4}+\rho s^2\bar{y}(x,s)=0 \tag{36}$$

where $\bar{y}$ denotes the Laplace transform of y, with the transformed boundary conditions as

$$\begin{aligned}
\bar{y}(0,s)&=0\\
I_h s^2\bar{y}'(0,s)-EI\bar{y}''(0,s)&=\tau(s)\\
M_p\bar{y}''(l,s)-EI\bar{y}'''(l,s)&=0\\
I_m s^2\bar{y}'(l,s)+EI\bar{y}''(l,s)&=0
\end{aligned}$$

Equation (36) has the general solution

$$\bar{y}(x,s)=A_1\sin\beta x+B_1\cos\beta x+C_1\sinh\beta x+D_1\cosh\beta x$$

where, $\beta^4=\rho s^2/EI$. The constants A_1, B_1, C_1 and D_1 must satisfy the boundary conditions

$$S_1(\beta)\begin{bmatrix}A_1\\B_1\\C_1\\D_1\end{bmatrix}=-\frac{1}{EI\beta^2}\begin{bmatrix}0\\\tau\\0\\0\end{bmatrix} \tag{37}$$

where, $S_1(\beta)$ has the same form as $S(\lambda)$ in equation (22).

Once the constants A_1, B_1, C_1 and D_1 and hence $\bar{y}(x,s)$ are known, it is possible to derive the transfer function from input torque to a particular output when the latter is expressed as a function of $\bar{y}$. It is clear from equation (37) that all the transfer functions that can be derived in this manner share a common denominator, this being the determinant of $S(\lambda)$. In practice, the resulting expressions are complex transcendental function of β. For the single-link manipulator with an end-point mass and hub inertia, the system poles are the roots of

$$D(\lambda) = |S(\lambda)| = 2(\sin\lambda\cosh\lambda - \cos\lambda\sin\lambda + 2\eta\lambda\sin\lambda\sinh\lambda) + 2\varepsilon\lambda^3[1 + \cos\lambda\cosh\lambda + \eta\lambda(\sin\lambda\cos\lambda - \sin\lambda\cosh\lambda)] \quad (38)$$

The numerator function $N(\lambda)$, on the other hand, depends on the particular output. From equation (37) and the definition of θ in equation (12), $N(\lambda)$ can be obtained as

$$N(\lambda) = -\frac{2}{EI\beta}(1 + \cos\lambda\cosh\lambda + \eta\lambda(\sinh\lambda\cos\lambda - \sin\lambda\cosh\lambda)) \quad (39)$$

If λ is a real root of $D(\lambda)$, then so are $-\lambda, j\lambda, -j\lambda$. The transfer function, expressed as the ratio of the numerator and the denominator functions above, are exact. This form, however, is not suitable for control design, as it requires explicit knowledge of the plant's poles and zeros. A more suitable form is obtained by replacing the numerator and denominator by their Maclaurin expansions, i.e.

$$D(\lambda) = \sum_{n=0}^{\infty} \frac{\lambda^n d^n D(0)}{n! d\lambda^n}$$

$$N(\lambda) = \sum_{n=0}^{\infty} \frac{\lambda^n d^n N(0)}{n! d\lambda^n}$$

As a consequence of the distribution of roots the Maclaurin expansions can be expressed as a product of quartic factors;

$$D(\lambda) = P_d(\lambda)\sum_{i=0}^{\infty}\left(1 - \frac{\lambda_i^4}{\lambda_{di}^4}\right)$$

$$N(\lambda) = P_n(\lambda)\sum_{i=0}^{\infty}\left(1 - \frac{\lambda_i^4}{\lambda_{ni}}\right)$$

where, P is a polynomial in λ of degree 3 or less. Using the relationship $\lambda^4 = -\rho s^2 l^4/EI$, the expression for the transfer function can be expressed in terms of the Laplace transform variable s. The final transfer function from the input torque to hub angle can thus be obtained as

$$\frac{\theta(s)}{\tau(s)} = \frac{1}{I_T s^2} \sum_{i=1}^{\infty} \frac{\left(1 + s^2/\omega_{ci}^2\right)}{\left(1 + s^2/\omega_i^2\right)} \tag{40}$$

Similarly, the transfer function from input torque to hub velocity $\dot{\theta}$ and end-point acceleration α can be written respectively as

$$\frac{\dot{\theta}(s)}{\tau(s)} = \frac{1}{I_T s} \sum_{i=1}^{\infty} \frac{\left(1 + s^2/\omega_{\alpha i}^2\right)}{\left(1 + s^2/\omega_i^2\right)} \tag{41}$$

and

$$\frac{\alpha(s)}{\tau(s)} = \frac{1}{I_T} \sum_{i=1}^{\infty} \frac{\left(1 - s^2/\alpha_{ti}^2\right)}{\left(1 + s^2/\omega_i^2\right)} \tag{42}$$

where, $\omega_{ci}, \omega_{\alpha i}$ and α_{ti} are real constants corresponding to the system zeros.

6 Experimentation

A schematic diagram of the experimental set-up is shown in Figure 2. This consists of an aluminium type flexible manipulator of physical dimensions and characteristics given in Table 1, driven by a high torque printed-circuit armature type motor. The measurement sensors consist of an accelerometer at the end-point of the manipulator for measurement of end-point acceleration, a shaft encoder and a tachometer, both at the hub of the manipulator, for measurement of hub angle and hub velocity respectively and four strain gauges located along the manipulator length at about $50mm$ (location-1), $250mm$ (location-2), $470mm$ (location-3) and $712mm$ (location-4) respectively from the hub. The outputs of these sensors as well as a voltage proportional to the current applied to the motor are fed to an IBM-AT compatible PC through a signal conditioning circuit and an anti-aliasing filter for analysis. The cutoff frequency of the anti-aliasing filter is set appropriately to satisfy the sampling requirements. In this process the measurement chain

is adjusted so that to achieve a good signal-to-noise ratio; the amplitude of the noise is kept within a level of $15mV$ with the signal level being within $10volts$.

An RTI-815 multi-function analogue/digital board is used as an I/O hardware unit. The board has a capacity of 8 differential analogue inputs, 2 analogue outputs, digital input and output and time related digital I/O functions. The analogue input channels each incorporate a 12-bit A/D converter with a conversion speed of 25μsec. The shaft encoder output is connected directly to the digital input port of the RTI-815 board. The analogue signals from the transducers, on the other hand, are connected to the analogue inputs of the board through the signal conditioning circuit and the anti-aliasing filter. A sampling period of $5ms$ is used which enables accommodating comfortably the first and second modes of vibration of the manipulator within the measurements.

In the experimental investigations to follow, two approaches for obtaining the required information are used: (a) the flexible manipulator system is excited by a random signal from a noise generator. The responses at various points are measured and fed to the computer through a set of amplifiers and filters. The collected data is then analysed to obtain the overall frequency response function (FRF). (b) the manipulator system is excited by a stepped sine wave from a Solartron 1170 spectrum analyser and the response around the pole and zero frequencies obtained. Here measurement is made only around the pole and zero frequencies with better resolution. The total FRF plot is obtained by combining the two methods of measurement with considerable accuracy.

6.1 Natural frequencies

To obtain the natural frequencies of vibration of the flexible manipulator system, two methods are introduced and their utilisation explored. The first method is based on the measurement of the autopower spectral density of the response of the system. This is referred to as the spectral density method. The second method is based on the measurements of the FRF and coherency function of the system. This is referred to as the FRF method.

The autopower spectral density $S_{xx}(\omega)$ of a signal x is defined as

$$S_{xx}(\omega) = S_x(j\omega)S_x^*(j\omega) \tag{43}$$

where $S_{xx}(\omega)$ is a real valued function containing the magnitude information only, $S_x(j\omega)$ is the linear spectrum of x given by the Fourier transform of the time signal $x(t)$. $S_x^*(j\omega)$ is the complex conjugate of $S_x(j\omega)$.

The response of the system can alternatively be described by the frequency response function. The equations relating the response of a system in random vibrations to the excitation are given as (Cannon and Schmitz, 1984)

$$\begin{aligned} S_{yy}(\omega) &= |H(j\omega)|^2 S_{xx}(\omega) \\ S_{xy}(j\omega) &= H(j\omega)S_{xx}(\omega) \\ S_{yy}(\omega) &= H(j\omega)S_{yx}(j\omega) \end{aligned} \tag{44}$$

where, $S_{xx}(\omega)$ and $S_{yy}(\omega)$ are the autopower spectral densities of the excitation signal x and the response signal y respectively. $S_{xy}(j\omega)$ and $S_{yx}(j\omega)$ are the cross-spectral densities between these two signals and $H(j\omega)$ is the FRF of the system. Let $H_1(j\omega)$ and $H_2(j\omega)$ denote two estimates of the FRF obtained according to the relations in equation (44) as

$$H_1(j\omega) = \frac{S_{xy}(j\omega)}{S_{xx}(\omega)} \quad \text{and} \quad H_2(j\omega) = \frac{S_{yy}(\omega)}{S_{yx}(j\omega)} \tag{45}$$

The error between the two functions is given by the coherency function defined as

$$\gamma^2(\omega) = \frac{H_1(j\omega)}{H_2(j\omega)} \tag{46}$$

In this manner, the coherency function gives a measure of the estimation error and indicates the level of coherence between the input and the output. If γ^2 is unity at some frequency ω this means that the output is entirely due to the input at that frequency. A

value of γ^2 less then unity, however, means that either the output is due to the input as well as other inputs or the output is corrupted with noise. When analysing the extracted signal, it is not sufficient to compute the Fourier transform of the signal. Instead an estimate for the spectral densities and correlation functions could be obtained, which are used to characterise the extracted signal. Although, these are computed from the Fourier transform, additional considerations are required concerning their accuracy and statistical reliability. It is necessary to perform an averaging process, involving several samples of the measurement, before a result is obtained. The two major factors which determine the number of averages required are the statistical reliability of the results and the removal of random noise from the signal (Newland, 1975; Bendal and Piersol, 1971). To overcome the leakage problem a Hanning type window function is employed before processing each block of data. MATLAB is used here to analyse the data and obtain the FRF, autopower spectral density and the coherency function (Little and Shure, 1988). This incorporates the use of an averaging method to remove the noise associated with the signal.

As the first few modes of the manipulator dominantly characterise the system behaviour, the parameters associated with the first two modes are extracted only. The flexible manipulator system is, thus, excited uniformly over a frequency range of 0-50 Hz, which covers the first two resonance modes. Autopower spectrum and frequency response function are obtained with a resolution of 0.488 Hz in the frequency range of 0 to 50 Hz. Measurement of the response near the pole and zero frequencies, for such a lightly damped flexible manipulator system, however, requires better resolution for spectral analysis. This, in turn requires large amounts of data, higher system memory and longer computation time. To cope with these issues, the response near the pole and zero frequencies is measured using the Solartron 1170 spectrum analyser where the manipulator is excited by a stepped sine wave, with a frequency resolution of 0.001 Hz.

The system was excited using a random signal as the input, and the time response of the system was measured at various locations in the system. This included the angle and velocity at the hub using a shaft encoder and a tachometer, at locations 1-4 along the manipulator using four strain gauges and at the end-point of the manipulator using an

accelerometer. The time history of the torque at the hub and the corresponding frequency distribution are shown in Figure 3. The autopower spectral densities of the signals thus measured were obtained using equation (43). These are shown in Figures 4 to 10 accordingly. The system was then excited using a random signal as the input, and the time-response of the system was measured, as before, at the hub, at the four locations (1-4) along the length of the manipulator and at the end-point. These were used to obtain the FRFs and coherency functions between the input torque and the responses using equations (45) and (46). These are shown in Figures 11 to 17. The pole and zero frequencies of the flexible manipulator system for the first two modes as obtained by identifying the peaks (maxima) and valleys (minima) in the autopower spectral density functions (Figures 4 to 10) and the FRFs (Figures 11 to 17) are shown in Tables 2 and 3 respectively with the corresponding analytical values.

For better accuracy to be achieved near the pole and zero frequencies, the system was excited with a stepped sinusoid from the spectrum analyser with a higher resolution. The input and output measurements of the system were used in the spectrum analyser to obtain the FRF around the pole/zero regions. The complete frequency response function is then obtained by combining the response with random excitation and the stepped sinusoid excitation. Table 4 shows the values of pole and zero frequencies as obtained using the spectrum analyser with a higher level of accuracy. The difference between the values obtained for pole and zeros using random excitation and stepped sinusoid excitation demonstrate the need for higher resolution around the pole and zero frequencies during the measurement of FRF. The pole and zero frequencies thus obtained using the spectrum analyser will be used in subsequent calculations.

It follows from Figure 3 that the flexible manipulator system is uniformly excited in the frequency range of interest (0-50 Hz). This is important in a system identification process. Tables 2 and 3 show the extraction of pole and zero frequencies from autopower spectrum and the FRF. As seen a reasonable level of accuracy is achieved in almost all cases. However, with a frequency resolution of the order of 0.488 Hz used in the digital

analysis program, further accuracy in obtaining the pole and zero frequencies is not achievable.

For the measurement at strain gauge positions (Figures 13 to 16) the coherence is almost perfect with small deviations. With the hub angle and hub velocity measurement, however, the coherence shows some error around the pole frequencies (Figures 11 and 12). With the acceleration measurement at the end-point the coherence shows some error at the lower frequency range (Figure 17). There are various reasons for the coherence not to be unity. These include

(a) Existence of noise on one or other of the two signals which could degrade the measured spectra near resonance. This is likely to influence the force signal so that $S_{xx}(\omega)$ becomes vulnerable, while at zeros it is the response signal which will suffer, making $S_{yy}(\omega)$. In the first of these cases, $H_1(\omega)$ will suffer the most and so $H_2(\omega)$ might be better indicator near resonance while the reverse applies at zeros.

(b) Possible problems arise when more than one excitation is applied to the structure. In this case, the response measured can not be directly attributed to the force which is measured. Such a situation can arise when the coupling between the structure and the excitation are not proper or there might be some form of constraint to the movement of the structure.

(c) Low coherence arises when the structure is not completely linear. Here again, the measured response can not be completely attributed to the measured excitation.

(d) A low coherence can arise in a measurement when the frequency resolution for analysis is not high enough to describe adequately the very rapidly changing functions such as are encountered near the poles and zeros on lightly damped structures. This is known as bias error.

In the measurements above it was found that low coherence occurred around pole and zero regions. It is more likely that this is mostly due to the lower frequency resolution of the analysis program and partly due to the non-linearity of the structure. As the frequency

response was measured near the pole and zero regions with better accuracy using the spectrum analyser, it is observed that there is a small variation in pole and zero frequencies with the location of measurement. Note that the error in the pole frequencies decreases with increasing the distance between the excitation of the structure and the response measurement location. This is because the two corresponding vibration modes of the structure become more pronounced in amplitude along the length of the manipulator with distance from the hub. The error trend in the zero frequencies, on the other hand, is variable with varying the distance between the excitation and measurement point.

It follows from the transfer functions in equations (40), (41) and (42) that the poles and zeros of the manipulator are functions of the loading conditions. Equations (38) and (39) accordingly indicate that the system poles, or natural frequencies, are functions of both the hub inertia and payload whereas the system zeros are functions of payload mass. To investigate this further, the effect of payload on the poles and zeros of the system was studied at the hub. This was done by exciting the system with a random torque input and measuring the response at the shaft encoder with various payloads at the end-point. The response thus obtained is analysed, as outlined earlier, to obtain the FRF of the system and thus the pole and zero frequencies. Figures 18 and 19 show the first two poles and zeros of the flexible manipulator for varying values of the payload. As noted, the variation in each case is predominant for small payloads. The pole frequencies are found to approach to cantilever modes when the hub inertia increases. However, it is not always possible to change hub inertia with an experimental structure. These observations are important for flexible manipulators which undergo changes in payload while performing given tasks. This demonstrates that as the mass increases there will be a noticeable change in the response of the manipulator; increased inertia due to the additional load leads to a reduction in the overall displacement of the manipulator in a fixed time period. It follows from equation (39) that the hub angle zeros are functions of the payload mass but are independent of the hub inertia; the zeros correspond to no motion at the hub. As the payload increases the system zeros migrate from cantilever beam frequencies and converge to the corresponding natural frequencies of a clamped beam where the latter represents the theoretical limit as

the payload mass tends to infinity. These observations are important in the development of suitable control strategies for flexible manipulator systems.

6.2 Damping ratio

There are several possible forms of damping within the system. These can be classified into three groups, depending in the source: (a) The flexible manipulator itself has structural damping due to dissipation of energy within the manipulator material, (b) Viscous damping and Coulomb damping (stiction/friction) associated with the drive motor, (c) External effects such as primarily air resistance as the manipulator rotates.

Due to the lightly damped nature of the structure it is very difficult to determine the damping coefficients for the flexible modes. The Coulomb damping associated with the motor is a constant retarding torque which always acts in the opposite direction to the velocity of the manipulator. This is overcome by having a constant voltage bias in the input torque to result in a torque equal and opposite to the frictional torque. The sign of the bias voltage will vary according to the direction of motion of the hub. The damping due to air resistance is not considered in the experiment, however, a comparison of the model with the system reveals that this damping does not affect the total damping of the system significantly.

As discussed earlier, the accuracy in measuring the damping ratio for the type of lightly damped system under consideration is important. To achieve this, the Solartron spectrum analyser was used to measure the response of the system near the resonance region. A stepped sine input was used from the analyser itself to excite the system with a frequency increment of 0.001 Hz and the frequency response of the system was measured. The frequency response data was then used to draw a Nyquist plot from which the damping ratio can be obtained. The method is based on the principle that in the vicinity of a resonance, the behaviour of a system is dominantly determined by the corresponding resonance mode being observed (Mergeay, 1981). The damping ratios thus obtained using frequency-response measurements of the system from the torque input to hub angle, end-

point acceleration and the four strain gauge locations along the manipulator are shown for the first two modes in Table 5. In a similar manner as the natural frequencies, the damping ratios also show small variations with the measurement location. It follows from Table 5 that the damping ratio decreases as the measurement location moves further away from the hub of the manipulator, where excitation is applied. This also indicates the nonlinear behaviour of the system.

6.3 *Hub modal slope coefficient*

To obtain the hub modal slope coefficient, a method based on the construction of the system transfer function is utilised (Martin, 1978; Gevarter, 1970). The transfer function of a linear elastic structure can be built up of a set of (alternative) poles and zeros, the values of which can be obtained experimentally. Thus, the open-loop transfer function from torque input $\tau(s)$ to the hub angle $\theta(s)$ of the flexible manipulator can be expressed as

$$\frac{\theta(s)}{\tau(s)} = \frac{1}{I_T s^2} \prod_{i=1}^{n} \frac{\left[\frac{s^2}{\Omega_i^2} + 2\xi_i \frac{s}{\Omega_i} + 1\right]}{\left[\frac{s^2}{\omega_i^2} + 2\xi_i \frac{s}{\omega_i} + 1\right]} \tag{47}$$

where, ξ_i is the damping ratio for mode i , Ω_i is the frequency of the zero, and ω_i is the frequency of the pole corresponding to this mode with the zero frequency falling between two consecutive pole frequencies. Using the state-space model of the system, equations (34) and (35), the open-loop transfer function from the input torque to the hub angle can be written as

$$\frac{\theta(s)}{\tau(s)} = \frac{1}{I_T s^2} + \frac{1}{I_T} \sum_{i=1}^{n} \frac{[\phi_i'(0)]^2}{s^2 + 2\xi_i \omega_i s + \omega_i^2} \tag{48}$$

As the values of ξ_i, ω_i and Ω_i can be obtained using the procedure given in the previous section, the value of $\phi_i'(0)$ can be computed using equations (47) and (48). Note in equation (48) that the first term on the right-hand-side corresponds to the rigid body

motion and the second term corresponds to the flexible motion of the manipulator. The hub modal slope coefficients for the first two modes of the system as obtained using the parameters of the system given in Tables 1 and 4 and equations (47) and (48) are shown in Table 6.

6.4 Modal gain of end-point accelerometer

To obtain the end-point acceleration sensor modal gain, consider the system open-loop transfer function from input torque to end-point acceleration. This can be written as

$$\frac{\alpha(s)}{\tau(s)} = \frac{l}{I_T} + \frac{1}{I_T}\sum_{i=1}^{n} \frac{\phi_i''(l)\phi_i'(0)s^2}{s^2 + 2\xi_i\omega_i s + \omega_i^2} \tag{49}$$

where $\phi_i''(l)$ is the acceleration sensor modal gain. The first and second terms on the right-hand-side of equation (49) correspond to the rigid and flexible motions of the manipulator respectively. Evaluating the hub angle and end-point acceleration at a resonance frequency ω_i using equations (48) and (49) yields

$$\theta(j\omega_i) = \frac{1}{I_T}\frac{[\phi_i'(0)]^2}{2\xi_i j\omega_i^2}\tau(j\omega_i) \tag{50}$$

and

$$\alpha(j\omega_i) = -\frac{1}{I_T}\frac{\phi_i''(l)\phi_i'(0)}{2\xi_i j}\tau(j\omega_i) \tag{51}$$

Dividing equation (51) over equation (50) and solving for the end-point acceleration modal gain yields

$$\phi_i''(l) = \frac{\alpha(j\omega_i)}{\theta(j\omega_i)}\frac{\phi_i'(0)}{\omega_i^2} \tag{52}$$

Thus, the steady state peak-to-peak ratio of end-point acceleration to hub angle can be measured experimentally at each resonance frequency and used in equation (52) to obtain

the end-point acceleration sensor modal gain. The sign of the modal gain $\phi_i''(0)$ is determined by observing whether the end-point acceleration signal is in phase or out of phase with the shaft encoder signal. Using the estimated system parameters given in Table 6 and the measured frequency response data in equation (52) the corresponding end-point acceleration modal gains can be obtained. These are shown in Table 7.

6.5 Model validation

To evaluate the model reliability the output of the model is compared in this section with the response of the system using a bang-bang input torque. The system is first excited by the input torque and the system response, consisting of the hub angle, hub velocity and end-point acceleration, is measured. Figure 20 shows a comparison between the system and model inputs. The torque inputs applied to each the model and the system are principally the same. However, due to the amplifier behaviour and motor dynamics, the shape of the torque input to the system is slightly changed. The corresponding hub angle is shown in Figure 21. It is noted that the model response is slightly faster than the system response. However, the eventual (steady-state) angular displacement of the manipulator for the model and the actual system agree with one another very closely. The hub velocity for the model and the actual system are shown in Figure 22. It is noted that the overall behaviour is similar for both the model and the system. However, some abruptness in the system behaviour at the half way and at the end of the movement is observed. As seen in Figure 23, the system and model response for the end-point acceleration in general agree with one another very closely, during the transient as well as steady-steady periods. A number of factors contribute to the occasional slight disagreements in magnitudes of the responses noticed at some points. The model, for instance, is a reduced-order one in which only the first two modes are included. The torsion and vertical motion as well as higher modes are not accounted for in the model. The effects of these, however, are present in the response of the actual system. Moreover, friction losses and dynamics of the motor which can considerably affect the system response, are not accounted for in the model. Note

further that the input torque appearing at the hub of the flexible manipulator is not exactly the same as the model input torque; a ringing effect and time delay during the change of state of the system torque input is observed. However, the model response appears to agree with the system response reasonably well and to within acceptable limits.

7 Conclusion

An investigation into the development of a suitable model of a single-link flexible manipulator system has been presented. The Lagrange's equation and modal expansion method has been utilised in obtaining an analytical model of the system characterised by a set of infinite number of modes. It has been shown that, for practical purposes, it is useful to convert the infinite-dimensional model to a model based on a finite number of the natural modes. This has lead to a matrix differential form for the model which can be readily converted to state-space form. Careful choice of the truncation level based on the physical attributes of the system has been shown to yield a very good approximation to the behaviour of the full-order model over a limited frequency range.

Transfer function models of the system have also been obtained which are useful in frequency-domain controller designs for the system. It has been shown and experimentally demonstrated that these transfer functions vary with the payload conditions of the manipulator. A small change in payload can result in a significant change in the manipulator's natural frequencies which, in a control context, can lead to an excessive deterioration in the performance of a highly tuned control system.

An experimental procedure of identification of model of a flexible manipulator system has been presented and verified. This involves obtaining the FRF with various input-output positions through a measurement of the pole and zero frequencies, which are then used to extract the model parameters, such as hub modal slope coefficient and modal gain of end-point accelerometer and damping ratios. A reasonable degree of coherence is obtained for the measured FRFs. A linear model that approximates the flexible manipulator open-loop dynamics has been identified, which includes one rigid body mode and two flexible modes.

Good agreement between the model and system output has been shown, with small deviations due to the model order truncation and dynamic behaviour of the driving actuator.

8 References

BOOK, W. J. and MAJETTE, M. (1983). Controller design for flexible distributed parameter mechanical arms via combined state-space and frequency domain techniques, *Transactions of the ASME Journal of Dynamic Systems, Measurement and Control*, **105**, pp. 245-254.

BENDAL and PIERSOL (1971). *Random data: Analysis and Measurement Procedures*, Wiley Interscience.

BREAKWELL, J. A. (1980). *Control of flexible spacecraft*, PhD Thesis, Department of Aeronautics and Astronautics, Stanford University, USA.

CANNON, R. H. and SCHMITZ, E. (1984). Initial experiments on the control of a flexible one-link robot, *International Journal of robotics research*, **3**, pp. 62-75.

CLOUGH, R. W. and PENZIEN, J. (1975). *Dynamics of Structure*, McGraw-Hill Book Company, New York.

EWINS, D. J. (1985). *Modal Testing: Theory and Practice*, Research Studies Press Ltd., New York.

GEVARTER, W. B. (1970). Basic relations for control of flexible vehicles, *AIAA Journal*, **8**.

HASTINGS, G. G. and BOOK, W. J. (1987). A Linear dynamic model for flexible robotic manipulator, *IEEE Control Systems Magazine*, **7**, pp. 61-64.

HUGHES, P. C. (1987). Space structure vibration modes: How many exists ? Which ones are important, *IEEE Control Systems Magazine*, **7**, pp. 22-28.

KANOH, H., TZAFESTAS, S., LEE, H. G., and KALAL, J. (1986). Modelling and Control of Flexible Robot Arms, *Proceedings. 25th Conference on Decision and Control*, December 1986, Athens.

KOROLOV, V. V. and CHEN, Y. H. (1989). Controller design robust to frequency variation in a one-link flexible robot arm, *Journal of Dynamic Systems, Measurement and Control*, **111**, pp. 9-14.

LITTLE, J. N. and SHURE, L. (1988). *Signal Processing Toolbox for MATLAB*, The Math Works, Inc., USA.

MARTIN, G. (1978). *On the Control of Flexible Mechanical System*, Ph.D. Thesis, Department of Aeronautics and Astronautics, Stanford University, Stanford, USA.

MEIROVITCH, L. (1970). *Methods of Analytical Dynamics*, McGraw-Hill book company, New York.

MERGEAY, M. (1981). Theoretical background of curve fitting methods used by modal analysis, *6th Modal Analysis Seminar*, 23-25 September 1981.

MEYER, G. E. (1971). *Analytical Methods in Conduction Heat transfer*, McGraw-Hill book company, New York.

NAGATHAN, G. and SONI, A. H. (1986). Non-linear flexibility studies for spatial manipulators, *Proceedings of IEEE International Conference on Robotics and Automation*, 7-10 April 1986, San Francisco.

NEWLAND, D. E. (1975). *Random Vibrations and Spectral Analysis*, Longman Press, London.

RAKSHA, F. and GOLDERBERG, A. A. (1986). Dynamic Modelling of a Single-link Flexible Robot, *Proceedings of IEEE International Conference on Robotics and Automation*, 7-10 April 1986, San Francisco.

SILVA, J. M. M. and MALA, N. M. M. (1988). Single mode identification techniques for use with small microcomputers, *Journal of Sound and Vibration*, **124**, pp. 13-26.

TSE, F. S., MORSE, I. E. and HINKEL, R. T. (1987) *Mechanical Vibrations: Theory and Applications*, Allyn and Bacon Inc., USA.

USORO, P. B., NADIRA, R. and MAHIL, S. S. (1986). A finite Element/Lagrange approach to modelling lightweight flexible manipulators, *Transactions of ASME Journal of Dynamic Systems, Measurement and Control*, **108**, pp. 198-205.

Table 1: Physical dimensions and characteristics of the flexible manipulator.

Length, l	$960mm$
Thickness	$3.2004mm$
Width	$19.008mm$
Mass density per volume, ρ/a	$2710\,kg/m^3$
Young's Modulus, E	$7.11\times10^{10}\,N/m^2$
Area moment of inertia, I	$5.1924\times10^{-11}\,m^4$
Hub inertia, I_h	$5.86\times10^{-4}\,kgm^2$
Manipulator moment of inertia, I_b	$0.0495kgm^2$

Table 2: Comparison of the pole frequencies obtained analytically and experimentally.

Experimental Method	Location	Pole 1 (12.499 Hz)		Pole 2 (36.36 Hz)	
		Measured (Hz)	Error (%)	Measured (Hz)	Error (%)
Autopower Spectra	Shaft encoder	11.719	6.24	37.109	2.06
	Tachometer	12.207	2.34	36.133	0.76
	Location-1	11.719	6.24	35.156	3.31
	Location-2	12.207	2.34	35.645	1.97
	Location-3	12.207	2.34	36.133	0.76
	Location-4	12.207	2.34	36.133	0.76
	Accelerometer	12.207	2.34	35.645	1.97
	Average	12.068	3.35	35.993	1.01
Transfer function	Shaft encoder	12.207	2.34	36.133	0.76
	Tachometer	12.207	2.34	36.133	0.76
	Location-1	11.719	6.24	36.133	0.76
	Location-2	12.207	2.34	36.133	0.76
	Location-3	12.207	2.34	35.645	1.97
	Location-4	12.207	2.34	36.612	0.69
	Accelerometer	12.207	2.34	36.133	0.76
	Average	12.137	2.9	36.132	0.63

Table 3: Comparison of the zero frequencies obtained analytically and experimentally.

Experimental Method	Location	Zero 1 (2.871 Hz)		Zero 2 (17.994 Hz)	
		Measured (Hz)	Error (%)	Measured (Hz)	Error (%)
Autopower Spectra	Shaft encoder	2.93	2.06	17.08	5.08
	Tachometer	2.93	2.06	17.568	2.37
	Location-1	3.418	19.05	13.184	26.73
	Location-2	3.906	36.05	20.508	13.97
	Location-3	-	-	20.461	13.71
	Location-4	-	-	20.461	13.71
	Accelerometer	3.418	19.05	20.019	11.25
	Average	3.027	5.43	18.754	4.22
Transfer function	Shaft encoder	2.93	2.06	17.09	5.02
	Tachometer	2.93	2.06	18.066	0.40
	Location-1	3.418	19.05	13.184	26.73
	Location-2	3.906	36.05	20.508	13.97
	Location-3	2.93	2.06	21.973	22.11
	Location-4	2.93	2.06	21.973	22.11
	Accelerometer	3.418	19.05	20.02	11.26
	Average	3.209	11.77	18.973	5.44

Table 4: Pole and zero frequencies obtained using the spectrum analyser.

Location	Zero 1 (2.871 Hz)		Zero 2 (17.994 Hz)		Pole 1 (12.499 Hz)		Pole 2 (36.36 Hz)	
	M'sured (Hz)	Error (%)	M'sured (Hz)	Error (%)	M'sured (Hz)	Error (%)	M'sured (Hz)	Error (%)
Shaft Encoder	2.90	1.01	17.92	0.41	12.00	3.99	35.18	3.25
Tachometer	2.91	1.36	17.919	0.42	12.00	3.99	35.19	3.22
Location-1	2.91	1.36	17.923	0.39	12.00	3.99	35.19	3.22
Location-2	2.924	1.85	17.925	0.38	12.00	3.99	35.20	3.19
Location-3	2.931	2.09	17.928	0.37	12.025	3.79	35.42	2.59
Location-4	2.935	2.23	17.930	0.36	12.037	3.7	35.60	2.09
Accelerometer	2.96	3.1	17.942	0.39	12.05	3.59	36.00	0.99
Average	2.924	1.85	17.927	0.37	12.016	3.86	35.397	2.65

Table 5: Damping ratios obtained from responses at different locations.

Response location	Damping ratios (ξ_i)	
	Mode 1	Mode 2
Shaft encoder	0.029	0.170
Tachometer	0.027	0.168
location-1	0.027	0.162
location-2	0.026	0.162
location-3	0.020	0.159
location-4	0.018	0.1317
Accelerometer	0.018	0.084
Average	0.024	0.148

Table 6: Parameters of model of the flexible manipulator system.

Parameter	Mode 1	Mode 2
Zero, Ω_i	$2.924Hz$	$17.927Hz$
Pole, ω_i	$12.016Hz$	$35.397Hz$
Hub modal gain, $\phi_i'(0)$	4.03	2.36
Damping ratio, ξ_i	0.024	0.148

Table 7: Parameters of model of the flexible manipulator system.

Parameter	Mode 1	Mode 2
Zero, Ω_i	$2.924Hz$	$17.927Hz$
Pole, ω_i	$12.016Hz$	$35.397Hz$
Acceleration modal gain, $\phi_i'(l)$	-2.19	3.47
Damping ratio, ξ_i	0.024	0.148

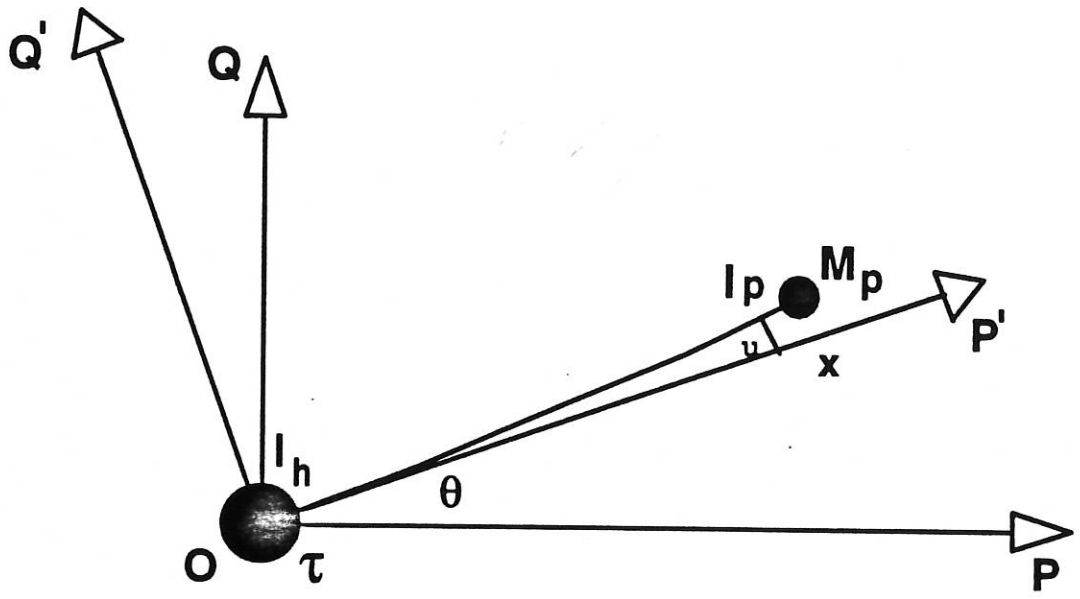

Figure 1: Schematic representation of the flexible manipulator system.

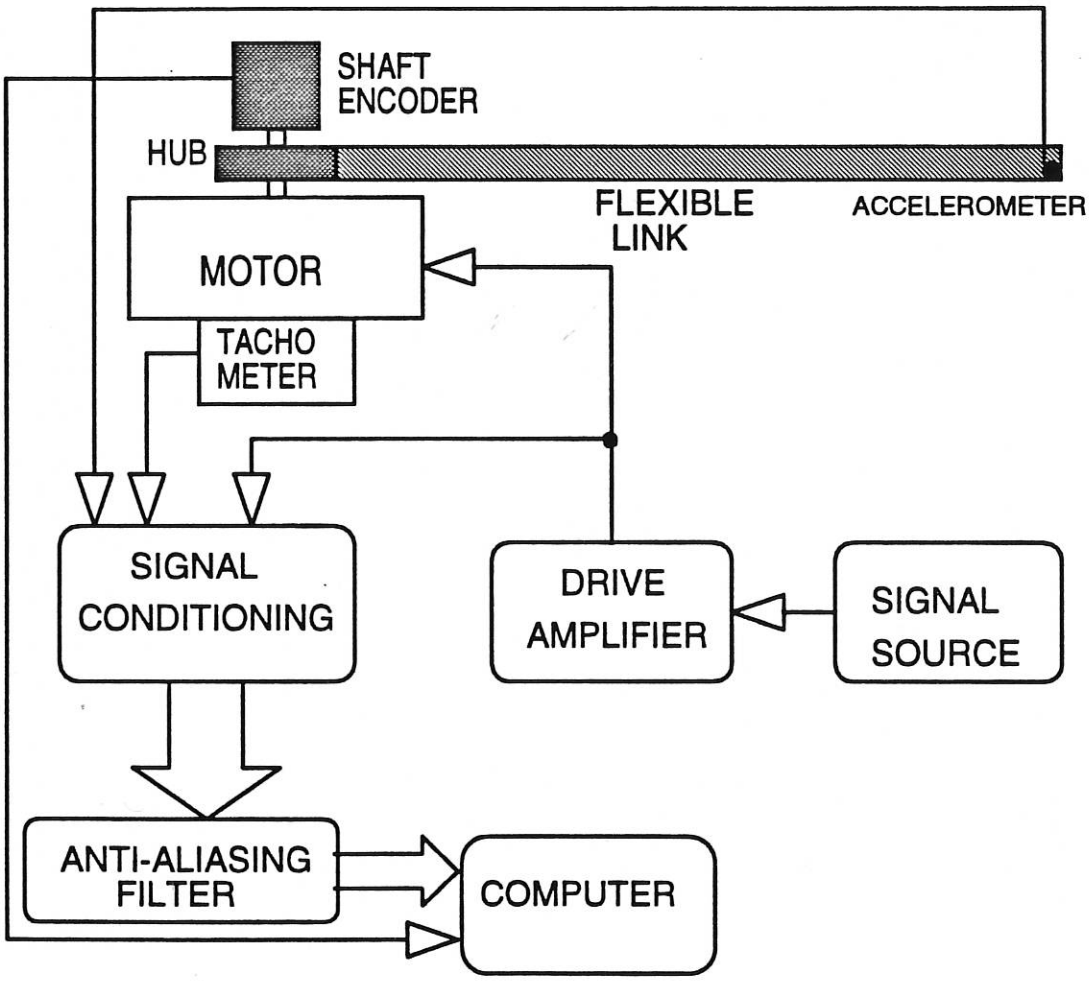

Figure 2: Experimental set-up for model parameter identification.

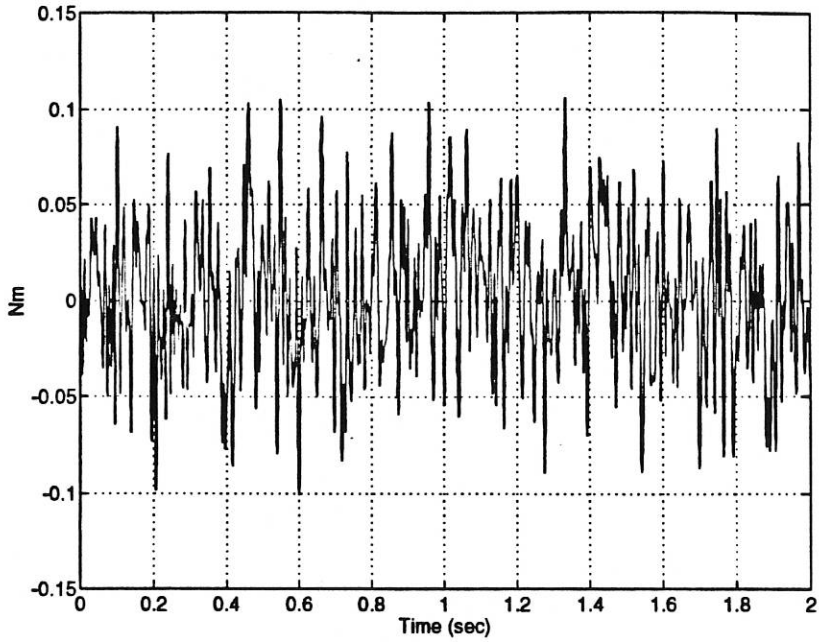

(a)

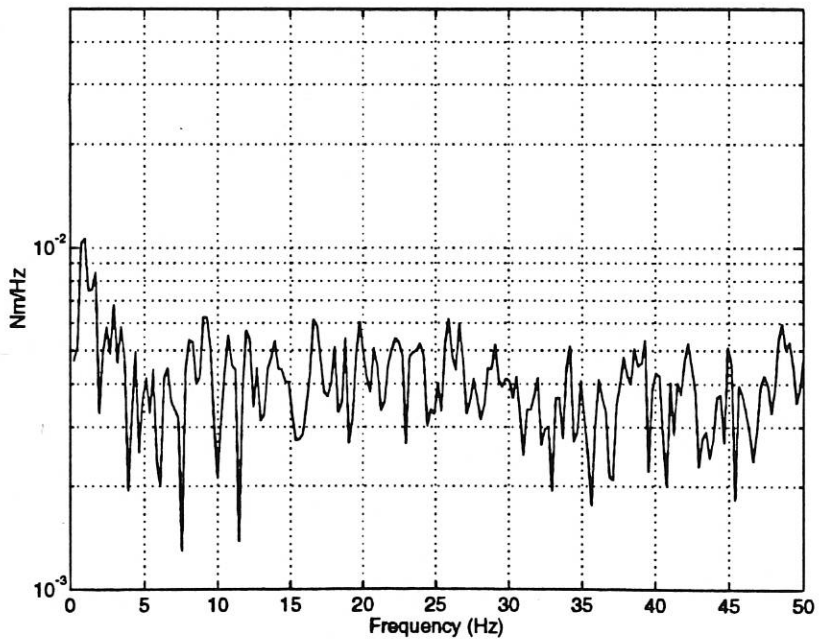

(b)

Figure 3: The random input torque;
(a) Time history.
(a) Spectral density.

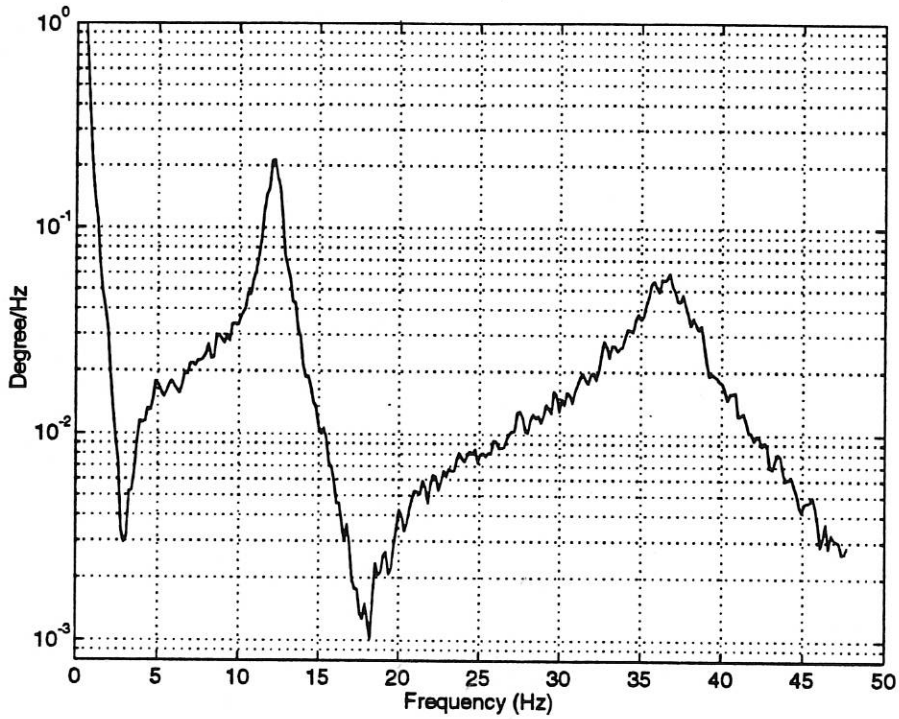

Figure 4: Autopower spectrum of the hub angle signal.

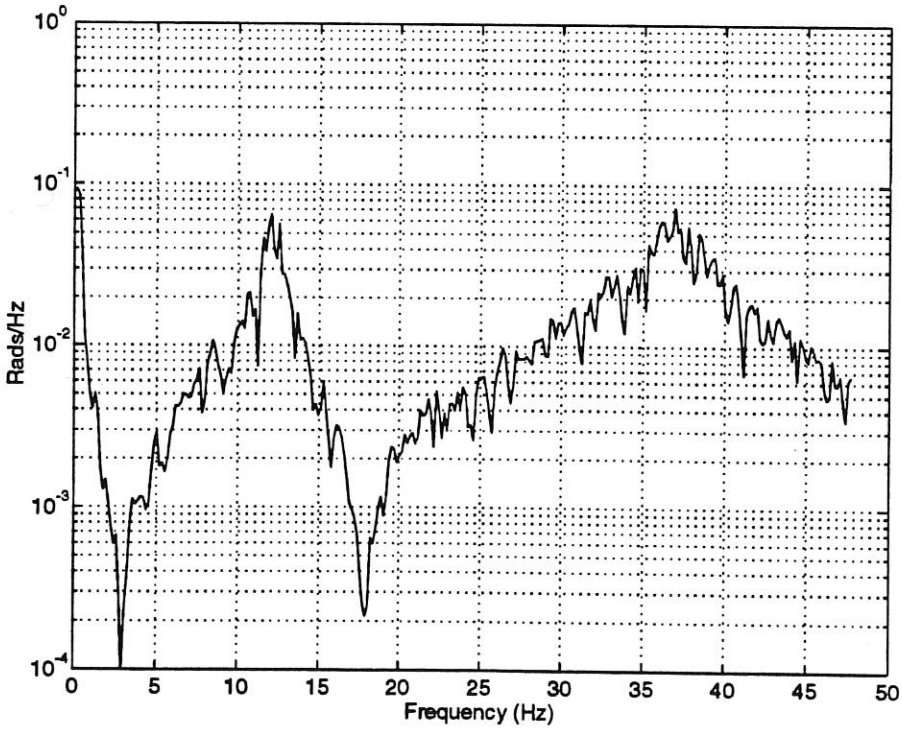

Figure 5: Autopower spectrum of the hub velocity.

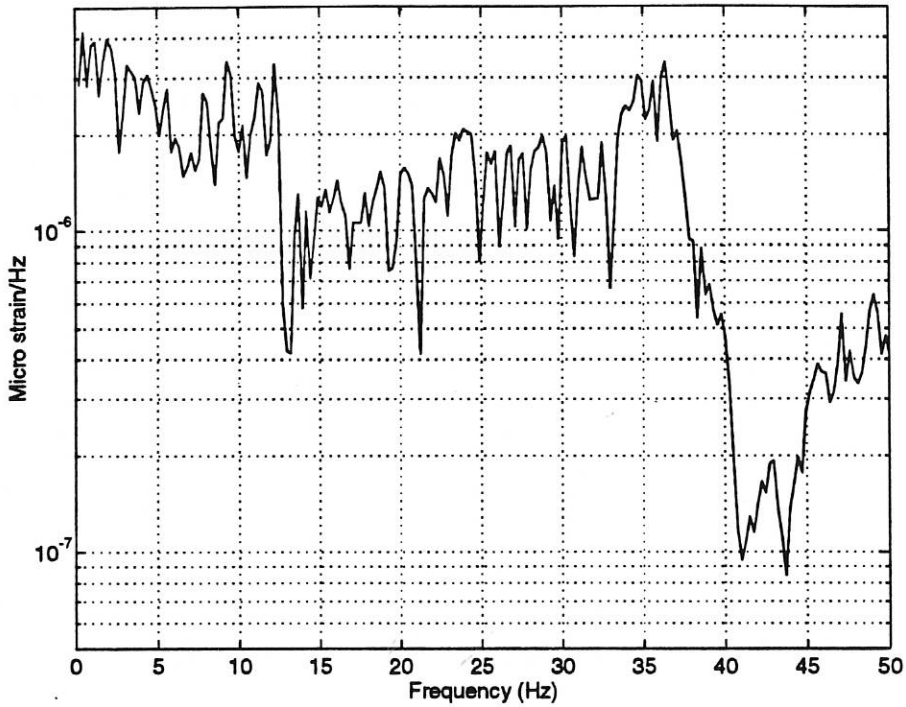

Figure 6: Autopower spectrum of strain gauge signal at location-1.

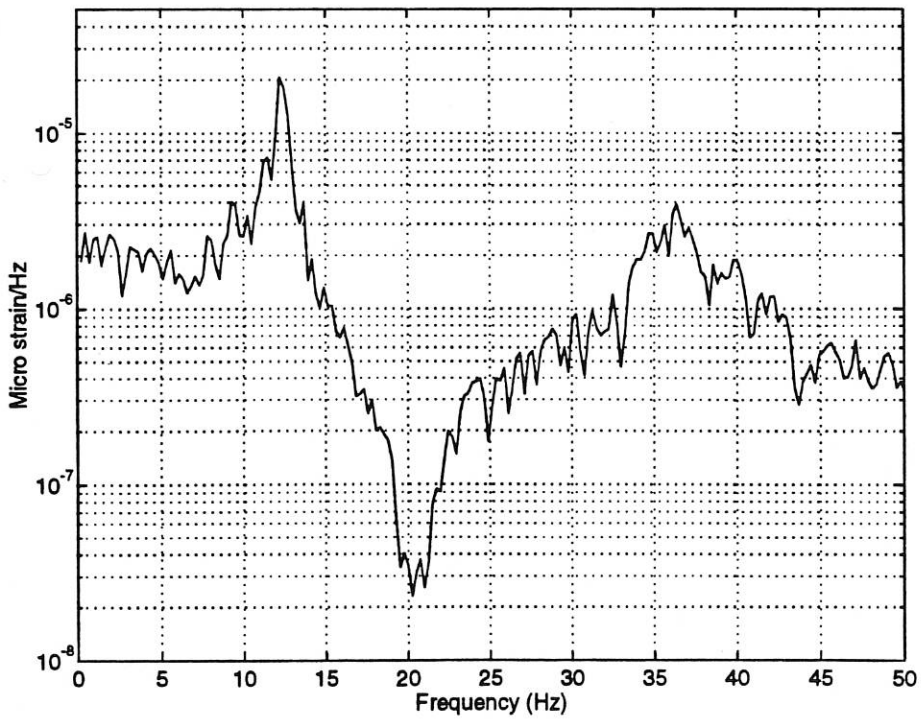

Figure 7: Autopower spectrum of strain gauge signal at location-2.

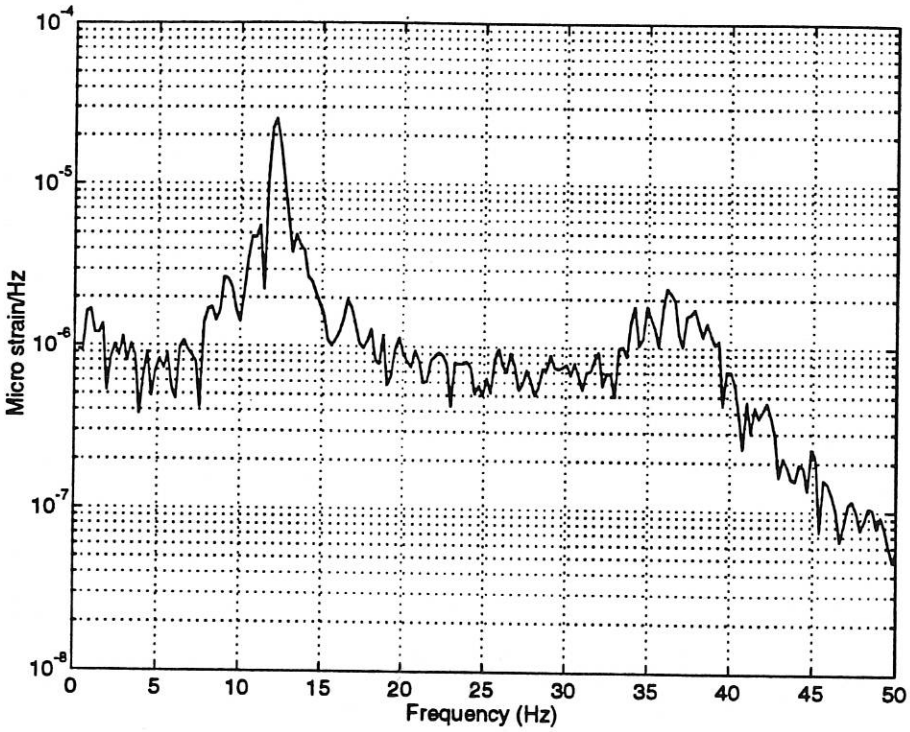

Figure 8: Autopower spectrum of strain gauge signal at location-3.

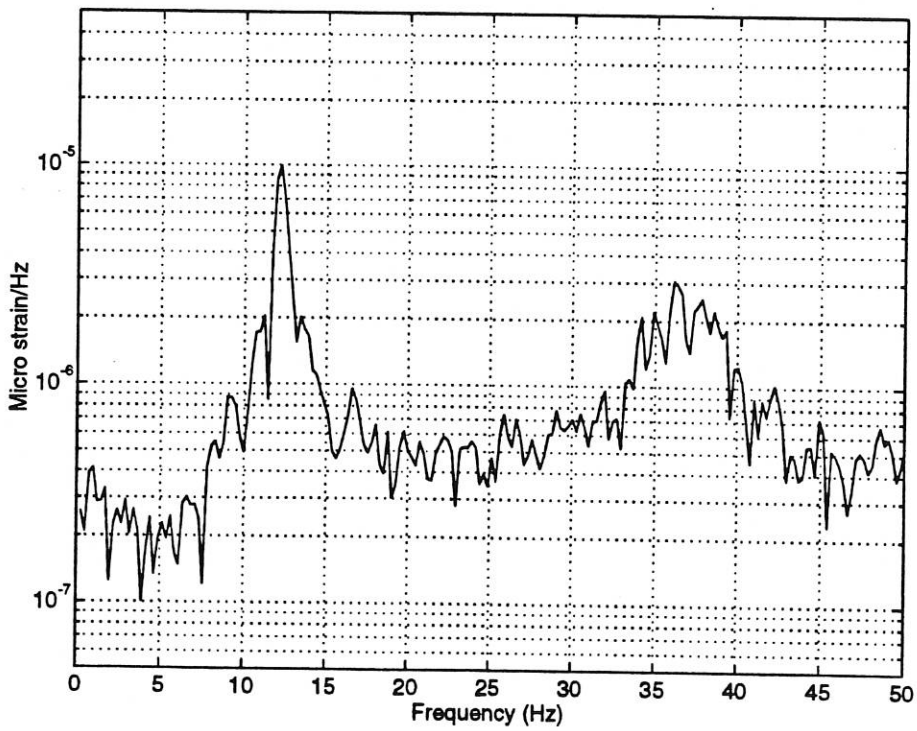

Figure 9: Autopower spectrum of gauge signal at location-4.

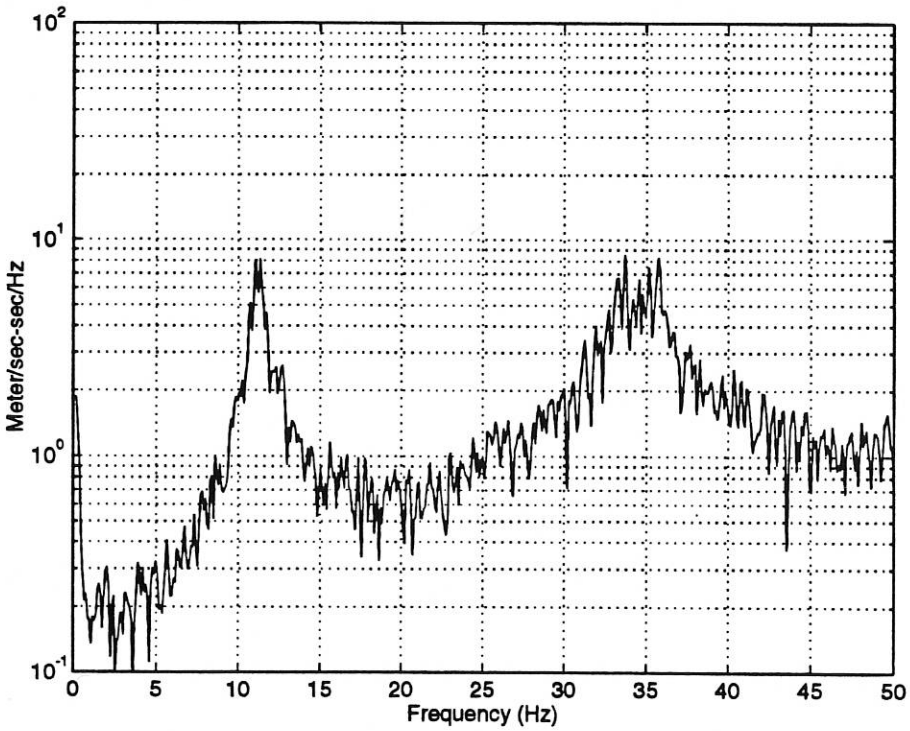

Figure 10: Autopower spectrum of the end-point accelerometer signal.

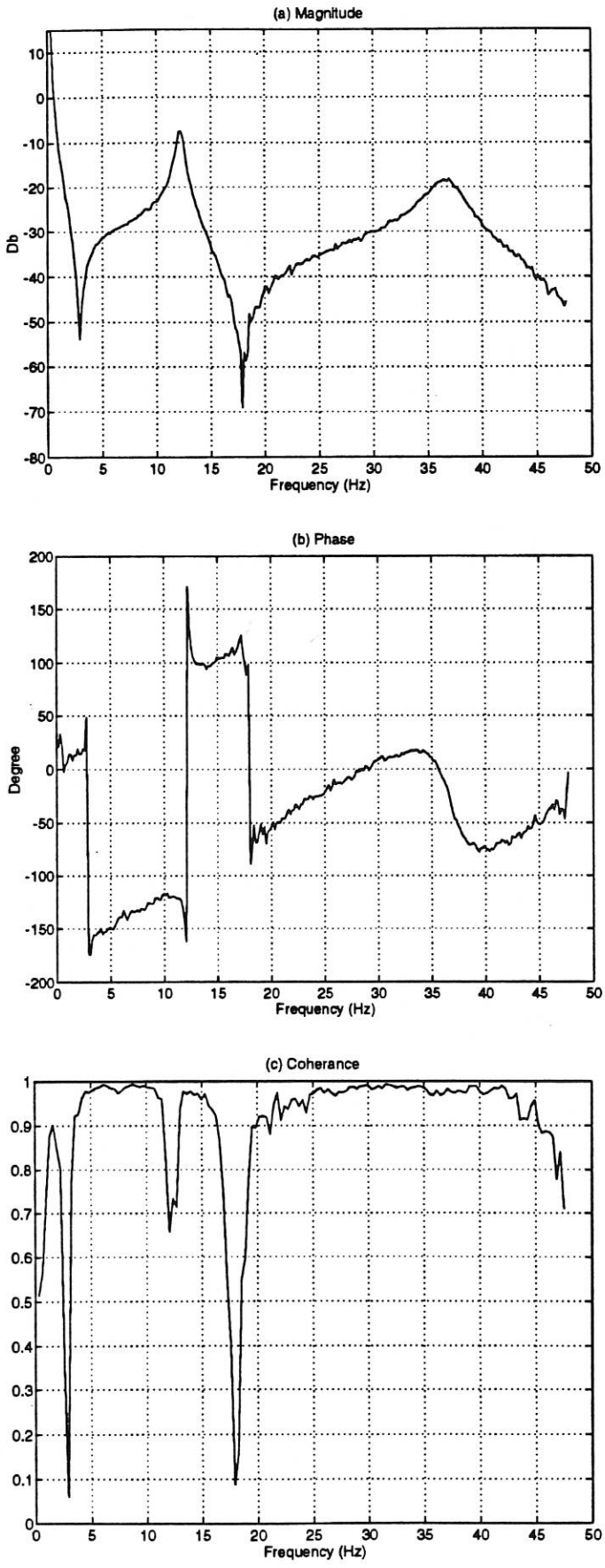

Figure 11: Frequency response function from torque input to shaft encoder output.

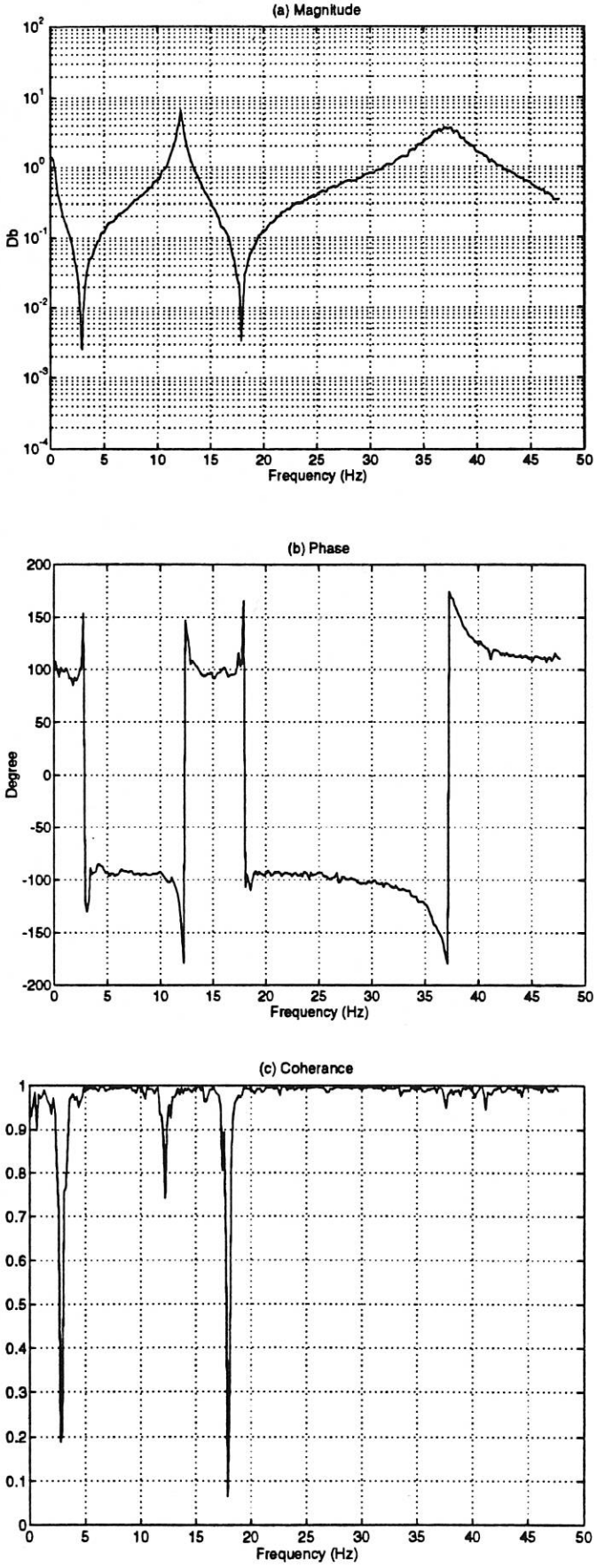

Figure 12: Frequency response function from torque input to tachometer output.

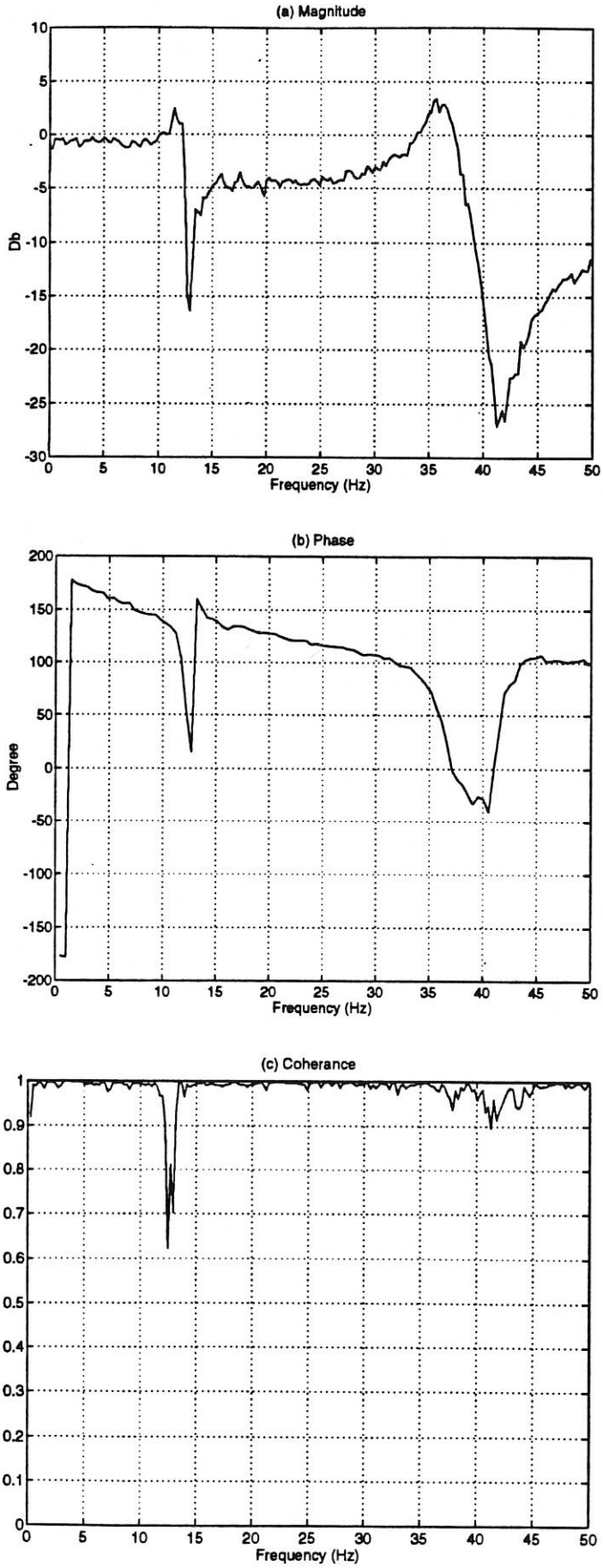

Figure 13: Frequency response function from torque input to strain at location-1.

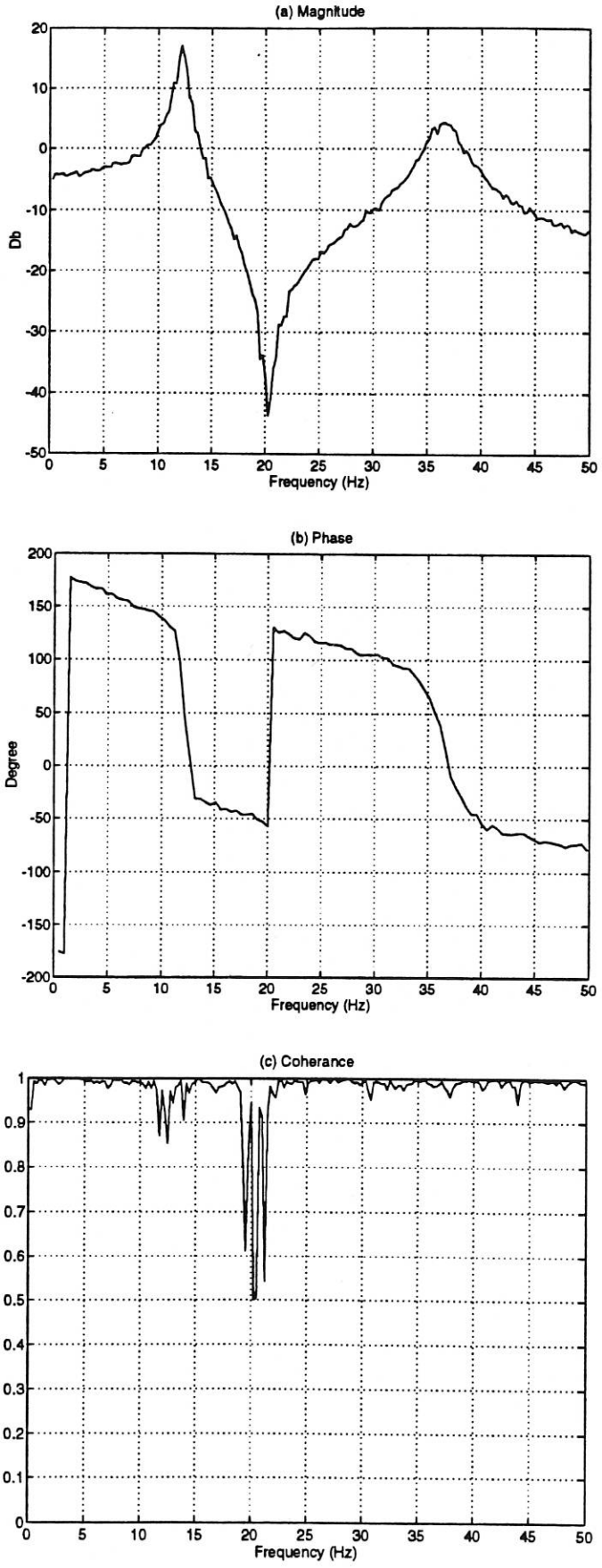

Figure 14: Frequency response function from torque input to strain at location-2.

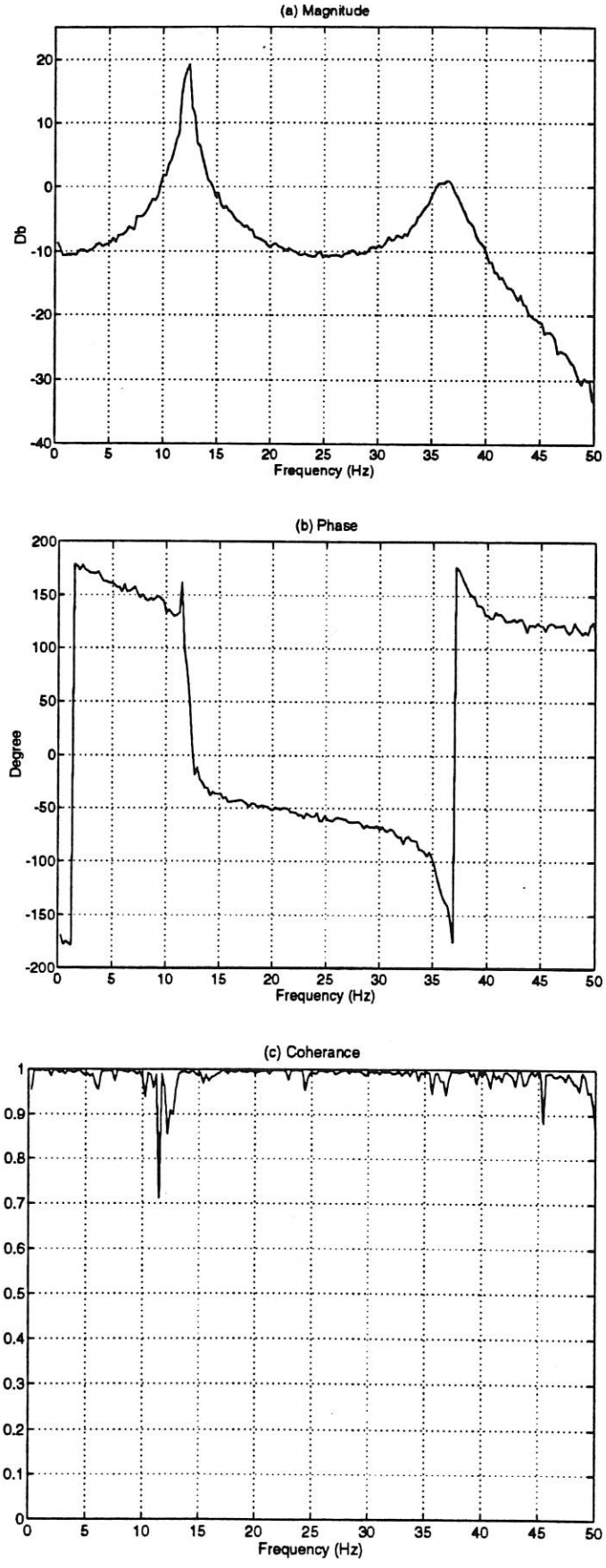

Figure 15: Frequency response function from torque input to strain at location-3.

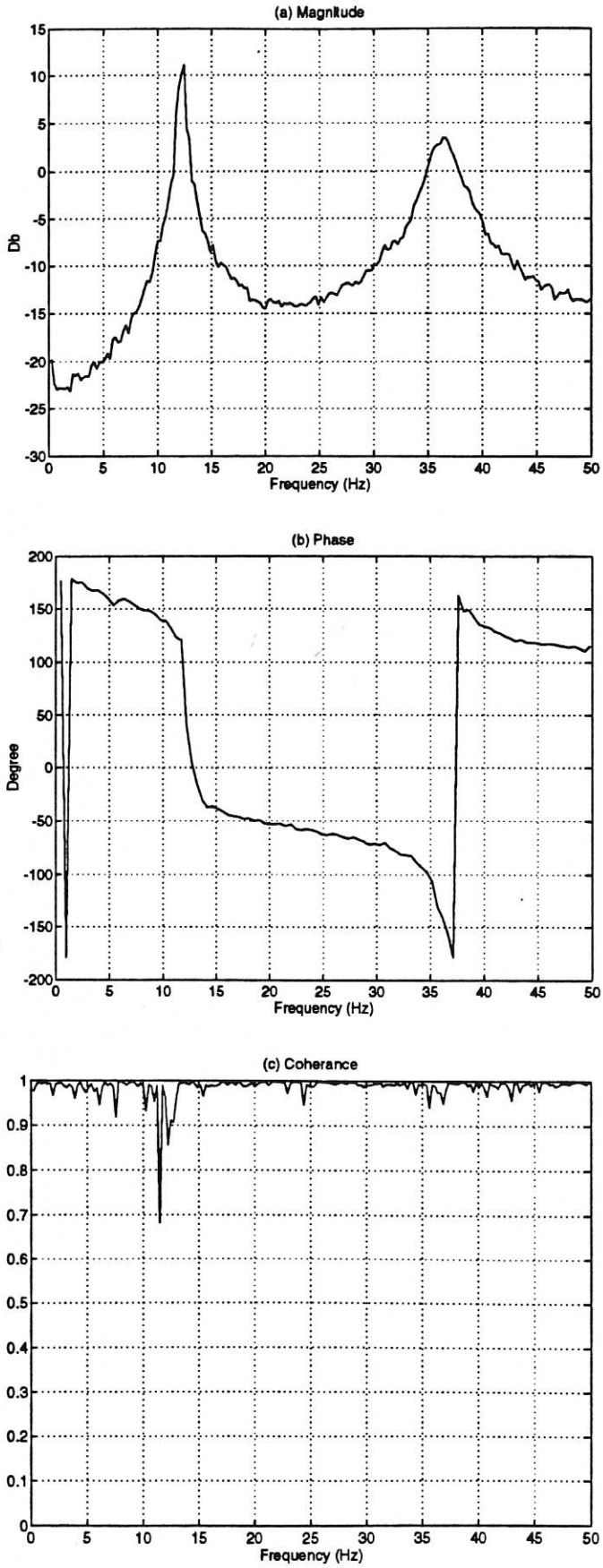

Figure 16: Frequency response function from torque input to strain at location-4.

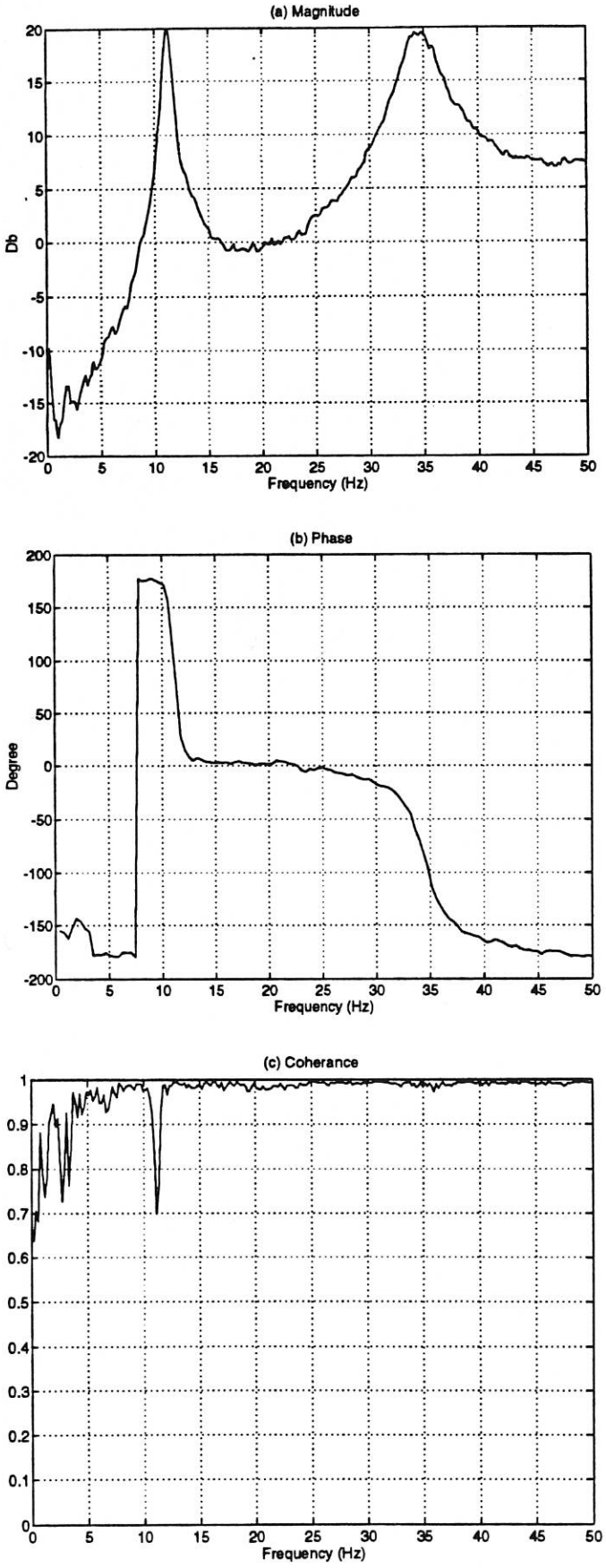

Figure 17: Frequency response function from torque to end-point acceleration signal.

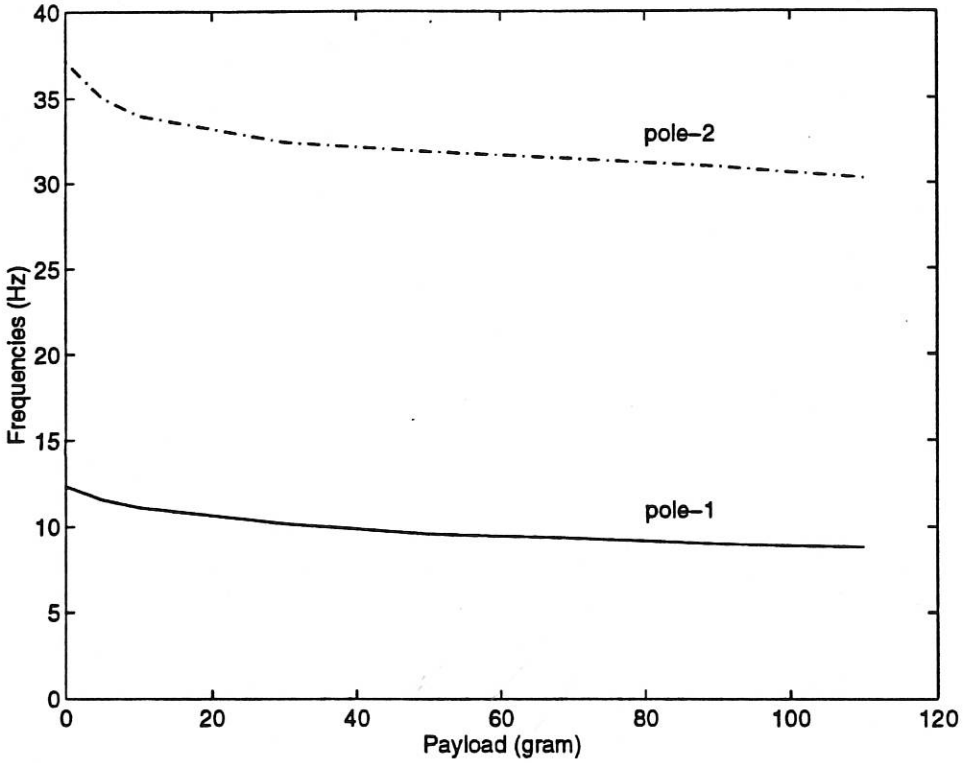

Figure 18: Variation of system poles with payload.

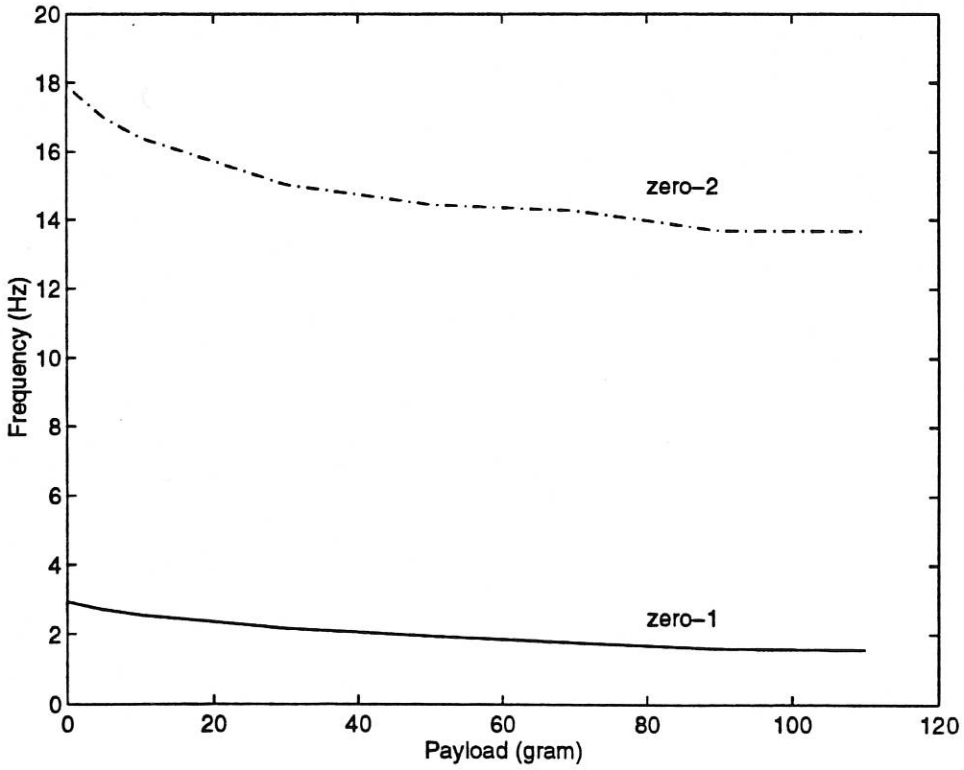

Figure 19: Variation of system zeros with payload.

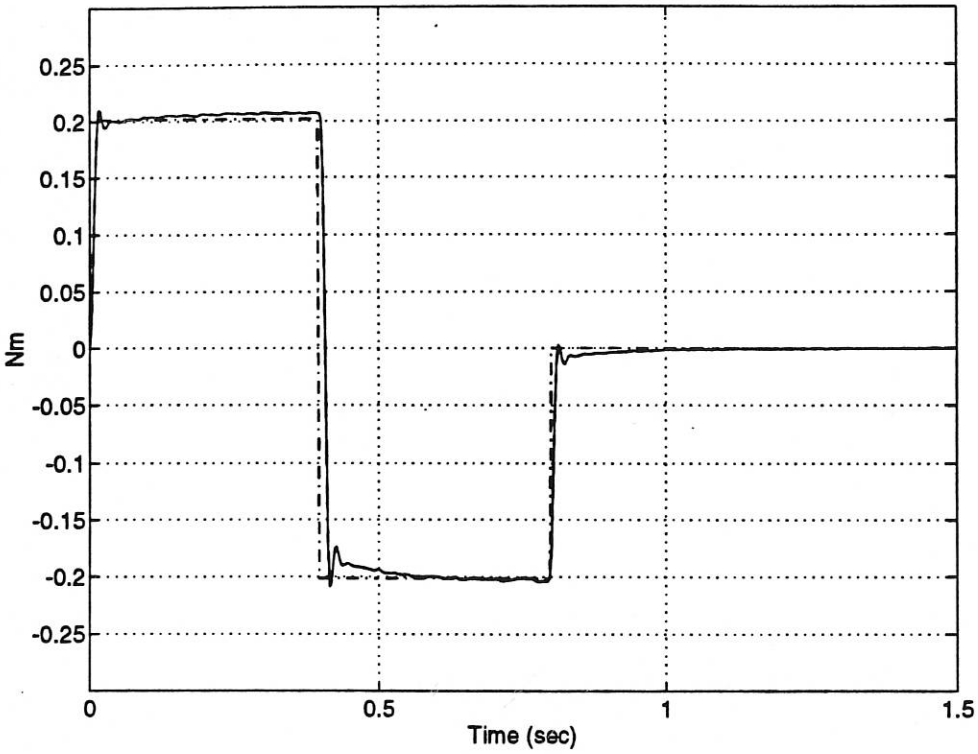

Figure 20: Torque input to the model (broken-line) and the system (solid-line).

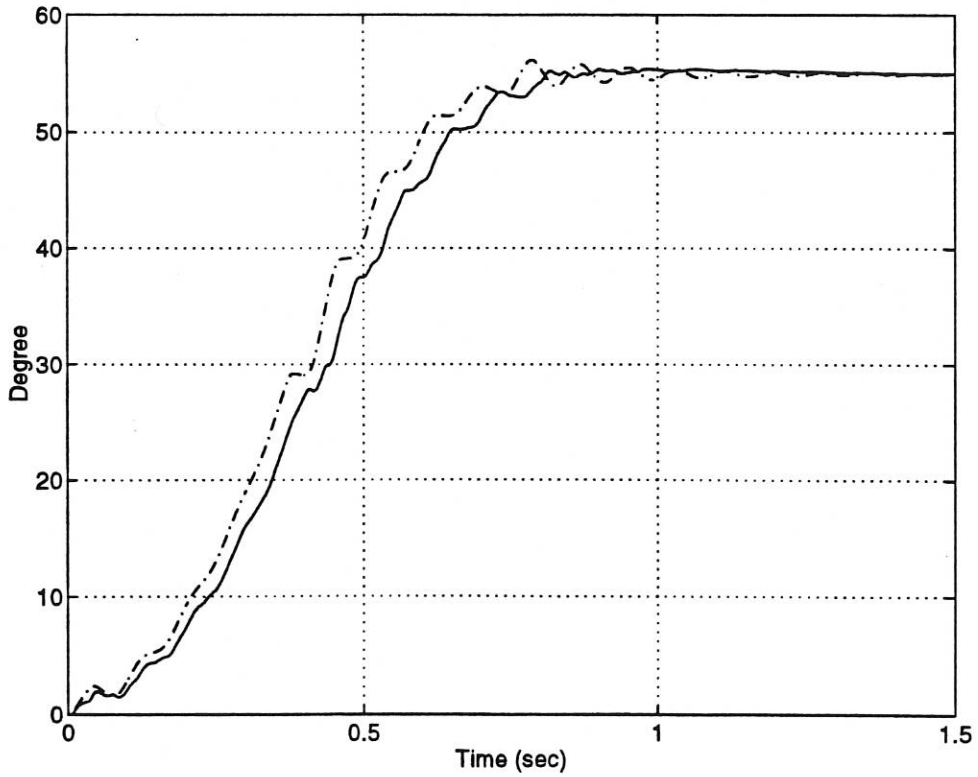

Figure 21: Hub angle for the model (broken-line) and the system (solid-line).

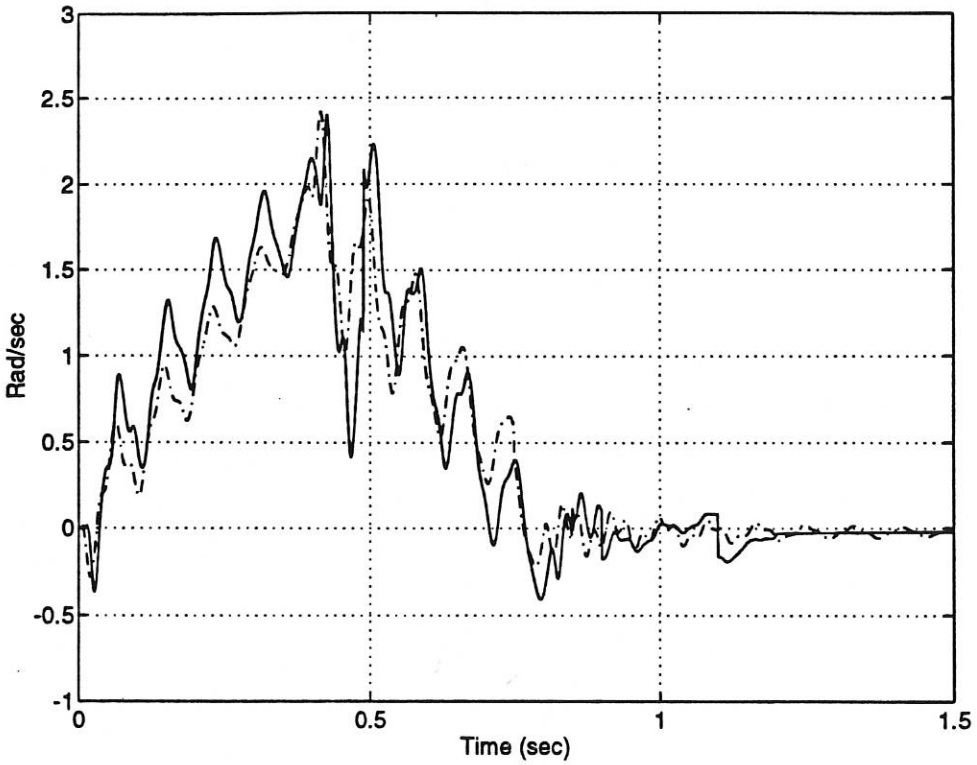

Figure 22: Hub velocity for the model (broken-line) and the system (solid-line).

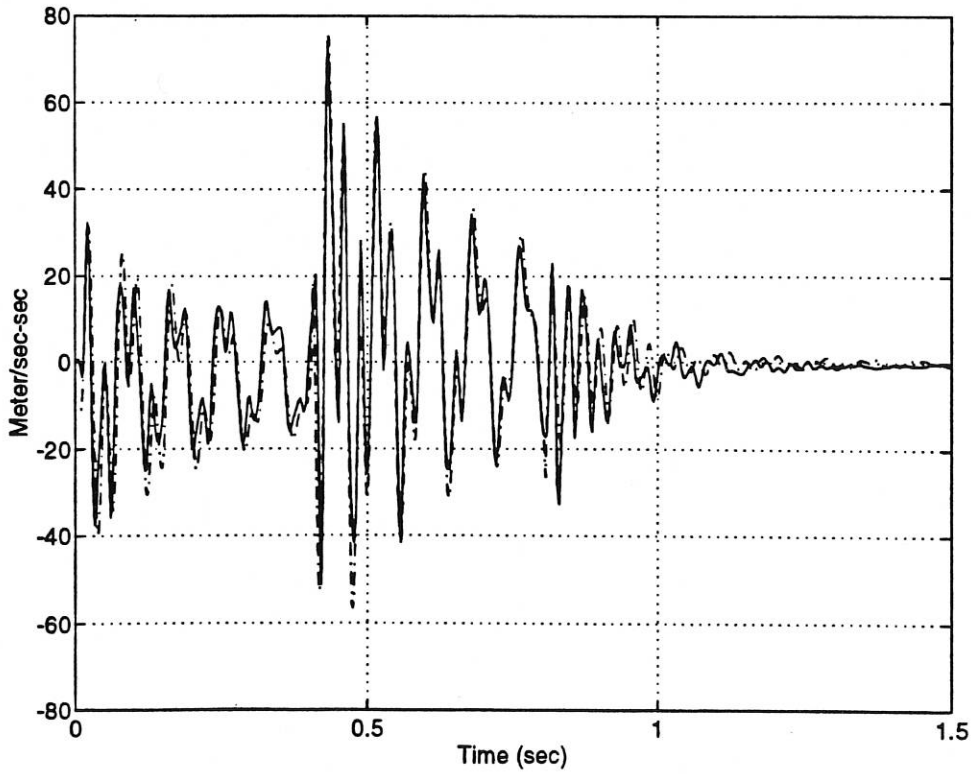

Figure 23: End-point acceleration for the model (broken-line) and the system (solid-line).